

Propagation of electron and proton shock-induced aurora and the role of the interplanetary magnetic field and solar wind

M. Meurant, J.-C. Gérard, C. Blockx, B. Hubert, and V. Coumans

Laboratoire de Physique Atmosphérique et Planétaire, Université de Liège, Liège, Belgium

Received 1 March 2004; revised 27 July 2004; accepted 11 August 2004; published 23 October 2004.

[1] Shock-induced aurora observed with satellite-borne ultraviolet imagers shows distinct characteristics from the more common and extensively studied aurora generated during magnetospheric substorms. It is initiated in the noon sector immediately following dynamic pressure pulses associated with the arrival of enhanced solar wind plasma at the front of the magnetosphere. The auroral brightening rapidly propagates toward the dawn and dusk sectors and may eventually trigger the development of an auroral substorm on the nightside. The FUV imaging system on board the IMAGE satellite has the ability to discriminate between proton and electron precipitation. This feature has been used to study the morphology and dynamics of the electron and proton precipitation following pulse-induced magnetospheric perturbations. A different dynamic is observed for aurora caused by electron and proton precipitation, as well as the important role played by the north-south component of the interplanetary magnetic field. The propagation from the noon to the night sector mainly occurs through the afternoon region for proton precipitation and the morning sector for electron aurora, as expected from azimuthal drift of newly injected plasma. The asymmetry of the precipitation distribution around the noon-midnight axis is more pronounced during negative B_z periods, when activity is the most important. The magnitude of both the interplanetary magnetic field and the solar wind speed appears well correlated with the precipitated power, by contrast with the solar wind density and the magnitude of the dynamic pressure, which appear to play a minor role. It is suggested that adiabatic compression and plasma waves play an important role on the locations of electron and proton precipitation in the dayside. *INDEX TERMS*: 2704 Magnetospheric Physics: Auroral phenomena (2407); 2784 Magnetospheric Physics: Solar wind/magnetosphere interactions; 2788 Magnetospheric Physics: Storms and substorms; 2451 Ionosphere: Particle acceleration; *KEYWORDS*: shock, pressure pulse, global imaging, solar wind, interplanetary magnetic field, propagation

Citation: Meurant, M., J.-C. Gérard, C. Blockx, B. Hubert, and V. Coumans (2004), Propagation of electron and proton shock-induced aurora and the role of the interplanetary magnetic field and solar wind, *J. Geophys. Res.*, 109, A10210, doi:10.1029/2004JA010453.

1. Introduction

[2] Forty years of auroral studies have shown that pressure pulses associated with coronal mass ejections (CME) can induce magnetospheric perturbations and auroral precipitation. *Nishida* [1978] showed that variations in solar wind dynamic pressure alter the magnitude and distribution of currents around and within the magnetospheric cavity. This feature manifests itself by strong variations of the magnetic field at the Earth's surface within 1 min after the shock on the magnetosphere. Using riometers and balloon-borne X-ray detectors, *Brown et al.* [1961], *Matsushita* [1961], *Ortner et al.* [1962], *Ullaland et al.* [1970], and *Vorob'yev* [1974] detected an immediate response to shock impacts in the form of increased energetic (tens of keV) electron precipitation and enhanced auroral luminosities

along the auroral oval. The enhancement observed by these authors lasts ~ 3 to 10 min.

[3] Most of the studies mentioned above used the term storm "sudden commencement" to name the initial magnetic perturbation preceding negative bays. In agreement with *Zhou and Tsurutani* [2001], we use the term "shock" to identify the SW and IMF sudden perturbation causing auroral activity, since it is believed that shocks and storm sudden commencements are essentially equivalent.

[4] Several studies suggest an influence of solar wind (SW) and interplanetary magnetic field (IMF) on substorms. *Burch* [1972] has highlighted the importance of a southward interplanetary magnetic field period to trigger substorms. *Akasofu and Chao* [1980] argued that substorms that sometimes follow shock impacts result from an enhanced rate of direct energy transfer by the solar wind to the magnetosphere. They also showed that the magnitude of the energy transfer is mainly linked to the velocity of the solar wind (v) and the intensity of the magnetic field (B) for a defined direction of the IMF.

[5] These parameters influencing substorm also influence shock-induced activity. The state of the magnetosphere a short time before the arrival of a shock (defined by the preconditioning due to solar wind and interplanetary magnetic field parameters) is important in determining the magnetospheric response. Since the shocks affect a large region of the magnetosphere, more magnetospheric regions act as sources for auroral precipitation than during isolated substorms. Global imaging with the Dynamics Explorer 1 (DE-1) satellite confirmed that a substorm may be triggered during the 30 min following a shock in a negative B_z period, while transpolar arcs are generally enhanced by a shock for positive B_z [Craven *et al.*, 1986]. In the case of sudden events with a short rise time, the magnetosphere does not have time to reach a steady state so that strong transient disturbances propagate in the magnetosphere. More recently, the availability of systematic measurements of auroral precipitation by Defense Meteorological Satellite Program (DMSP) and NOAA satellites and monitoring with global imagers such as POLAR-UVI and IMAGE-FUV added considerably to this field.

[6] The typical development of a shock-induced electron aurora begins by an enhanced activity in the noon sector. Within a few minutes, the region of enhanced auroral emission expands longitudinally at speeds ~ 6 to 11 km s^{-1} , reaching the dawn and dusk sectors and eventually the nightside oval. Zhou and Tsurutani [1999] matched the longitudinal propagation of the FUV aurora from noon to dawn and dusk with the speed of the pressure pulse moving tailward. The typical morphology of auroral activity triggered by shock arrivals is therefore very different from the evolution during substorms, as described by Chua *et al.* [2001]. Boudouridis *et al.* [2003] presented evidence of the preconditioning of the magnetosphere by the B_z sign, based on DMSP data, in agreement with the earlier study by Burch [1972]. The role of the preconditioning process was also confirmed by the Liou *et al.* [1998] study, which highlights the effect of the 60 min period of negative B_z preceding the shock on the precipitated power. Numerous studies [Heppner, 1955; Schieldge and Siscoe, 1970; Kawasaki *et al.*, 1971; Burch, 1972; Kokubun *et al.*, 1977; Akasofu and Chao, 1980] suggest the ability of shocks to trigger a substorm expansion phase on the nightside. Some of them established that this response depends on the intensity of the shock. Zhou and Tsurutani [2001] examined this correlation and highlighted the role played by the north-south component of the IMF. They argued that the ability of a shock to trigger a substorm is enhanced when the magnetosphere is preconditioned with a negative B_z value averaged over 90 min prior to the shock arrival. The mean energy of the precipitated electrons was also found lower during the shock-induced aurora ($E < 7 \text{ keV}$) than during isolated substorms [Chua *et al.*, 2001; Meurant *et al.*, 2003b].

[7] Several processes generated by the shock on the front and viscous interaction on the flanks probably cause auroral precipitation at different magnetic local times (MLT), magnetic latitudes (MLAT), and different times. On the basis of FAST and DMSP data, Tsurutani *et al.* [2001] and Zhou *et al.* [2003] examined possible processes to explain the global aspect of the magnetospheric perturbation. On the dayside auroral oval, adiabatic compression likely plays a major role at least as an initial step. Preexisting plasma on outer zone

magnetospheric field lines becomes betatron accelerated/energized following transfer of solar wind ram energy. By conservation of the first adiabatic invariant, $W_{\perp}/|B|$, where W_{\perp} is the particle perpendicular kinetic energy, magnetospheric compression causes an increase of W_{\perp} that leads to loss cone instabilities with growth of plasma waves and concurrent electron and proton pitch angle scattering. The shock can also trigger mechanisms inducing field-aligned currents that produce intense discrete electron aurora. Magnetic field shearing, Alfvén wave generation, fast mode waves carrying the pressure gradient and magnetic reconnection are also able to generate these currents, as explained below [Zhou *et al.*, 2003]. As shock pulses compress the magnetopause and propagate antisunward, the magnetic field lines in the magnetopause and magnetopause boundary layers may be dragged tailward with the shock. Therefore magnetic field shearing may occur between the distorted magnetic field lines at lower L shell. Haerendel [1994] has shown that this magnetic shearing can generate field-aligned currents due to the decoupling of plasma, allowing fast stress relief. The generation of the unstable field-aligned currents is a process that converts energy stored in magnetic shear stresses initiated from the shock compression into kinetic energy. In a context of compressible, nonviscous, and perfectly conducting plasma in a magnetic field, shear Alfvén waves may be generated. The plasma flow across the field increases the bending of the field and generates the shear Alfvén waves and field-aligned currents. Particles precipitated along these field-aligned currents eventually cause aurora so that the aurora would be observed at all latitudes where the shear Alfvén waves occur. It is not known at this time why field-aligned current and aurora would only occur in a limited latitudinal region, while these waves are generated in all L shells. Their propagation speed is $\sim 1000 \text{ km s}^{-1}$, which implies a propagation time to the nightside region on the order of 1 min [Zhou *et al.*, 2003]. Another way by which the shock perturbs the magnetosphere is the generation of fast mode waves carrying the pressure gradients able to generate currents in the ionosphere. Southwood and Kivelson [1990] predicted the creation of a pair of oppositely directed field-aligned currents into the ionosphere, whereas Glassmeier and Heppner [1992] argued that only one field-aligned current develops. This model explains the consistency between the SW speed and the antisunward propagation speed of auroral intensification [Zhou and Tsurutani, 1999]. Dayside magnetic reconnection occurs more intensely and frequently with interplanetary shocks pulses [Song and Lysak, 1989]. This mechanism which explains some of the energy transfer from the solar wind to the magnetosphere also accounts for the field-aligned current intensification at L shells that map to the poleward boundary of the dayside auroral oval. The currents should primarily occur near local noon where the solar wind hits the magnetopause. Since the reconnection rate is more important during negative B_z episodes, this effect is expected to be enhanced during these periods. As explained before, the B_z component of the IMF exerts an influence both on the preconditioning of the magnetosphere and on the rate of energy transfer by the solar wind to the magnetosphere. The impact of viscous-like interaction on the night sector was discussed by Liou *et al.* [1998].

[8] With the FUV instrument on board on the IMAGE satellite, a multispectral global view of the north aurora is obtained with a 2 min resolution. Two different imagers respond to the electron aurora (LBH for the WIC instrument and a narrow window centered on the OI 1356-Å emission for the SI13 imager). Doppler-shifted Lyman- α emission is isolated by the SI12 sensor to map the proton aurora. Using this imaging system, *Meurant et al.* [2003b] showed that the speed of MLT propagation from the noon sector to dusk and dawn may be different for electron and proton precipitation. At a given time, latitudinal boundaries of enhanced electron and proton precipitation may also be different. In this study, we examine, on the basis of combined IMAGE-FUV and Advanced Composition Explorer (ACE) satellite data, the behavior of electron and proton shock-induced aurora and its time evolution in different MLT sectors. We also analyze the influence of the SW and IMF parameters prevailing during the 10 min following the shock for cases of positive and negative B_z . Considering that the importance of the preconditioning has already been established by previous work, the correlation with SW and IMF parameters existing just after the shock is studied in order to assess the importance of a short time effect of these parameters on the shock induced activity which it produces. We first describe a typical case study for each orientation of B_z . We then present a statistical study of the temporal evolution of auroral electron and proton power injected in different magnetic local time sectors. We also determine the influence of the SW and IMF parameters on auroral precipitation during a short time period following the shock. Finally, we discuss mechanisms able to explain the observed characteristic temporal and spatial evolution.

2. IMAGE-FUV Observations of Shock Aurora

[9] For this study, we consider the 1 May 2000 to 31 December 2002 period during which the north polar region was optimally viewed by the FUV imagers. The shock events are selected on the basis of the SW dynamic pressure calculated using solar wind density and bulk velocity measured with the ACE satellite. The ACE satellite is well suited for its nearly constant position relative to the Earth. We define a shock as an event where the dynamic pressure measured by ACE increases by at least a factor of two during a period of time shorter than 15 min. The time delay between the detection of the shock by ACE (τ_{ACE}) and the arrival at the magnetopause is determined on the basis of the ACE position and the measured solar wind bulk speed. This time shift allows the determination of the arrival time of the dynamic pressure pulse on the front of the dayside magnetosphere. In order to permit a complete temporal and morphological analysis, the following criteria were met when selecting the events for this study. First, FUV data must be available from 15 min before to 30 min after the time when the SW shock buffeted the magnetosphere. Second, the region between 60° and 80° MLAT was in the field of view of the FUV instruments for all longitudes during the time period considered. Some of the cases meeting these conditions were rejected to avoid problems associated with too weak signals. In these cases, the dayglow contamination was too large relative to the auroral

signal so that the correct auroral contribution could not be accurately retrieved following dayglow subtraction algorithm as described below.

[10] The three FUV cameras obtain simultaneous images of the planet once every 2 min. The SI12 imager is sensitive to Doppler-shifted Lyman- α emission at 121.8 nm emitted by the beam of fast H atoms resulting from charge exchanges between auroral protons and atmospheric constituents. This imager provides global 5-s snapshots of the precipitation of protons carrying energy exceeding approximately 3 keV. The other spectral imager (SI13) isolates a 5-nm region centered on the OI line at 135.6 nm. Finally, the Wideband Imaging Camera (WIC) provides 10-s snapshots of auroral emission in the 135–180 nm region including N_2 LBH bands and NI lines [*Mende et al.*, 2000]. Dayglow subtraction has been applied to WIC and SI13 images to account for contamination of the dayside auroral signal [*Immel et al.*, 2000]. A small background subtraction is also applied to the SI12 image. The proton contribution to the WIC and SI13 signals is also removed, consistently with the proton flux determined from the SI12 pixels. Since atmospheric absorption by O_2 varies in the WIC and SI13 wavelength intervals, the ratio of these measurements is sensitive to the depth at which the precipitating particles cause optical emissions and thus is sensitive to the average energy of the particles. Consequently, simultaneous measurements of these two instruments can be used to estimate the electron average energy and energy flux [*Hubert et al.*, 2002; *Meurant et al.*, 2003a; *Coumans et al.*, 2004]. The proton energy flux is deduced from the SI12 image based on an assumption on the proton mean energy. For this study the local proton mean energy is provided by the *Hardy et al.* [1989] empirical model. Once the electron and proton energy fluxes are determined for each pixel, the global power is obtained by multiplying this flux by the pixel area and summing over the total auroral region. The area subtended by each pixel is calculated from the spacecraft pointing information.

[11] The time evolution of the auroral power incident in one hemisphere or in a limited MLT sector deduced from this method will be examined and correlated with the solar wind (dynamic pressure, P_{dyn} , solar wind speed, v , density, ρ) and IMF (magnitude of the magnetic field, B , vertical component of the magnetic field, B_z) parameters. To separate the contribution of the shock aurora from preexisting auroral signal and residual background contamination, we subtract the observed power in a particular sector averaged over a time period preceding the shock. This procedure assumes that the airglow signal is not modified during and after the shock. This assumption is justified by the relatively short period of time considered. The power calculated with this procedure is attributed to the sole interaction of the shock with the Earth's magnetosphere. Figure 1 shows an example of raw and corrected electron and proton hemispheric powers observed with the FUV imager on 18 March 2002 between 1302 and 1351 UT.

3. Cases Studies

3.1. Shock Event of 18 April 2001

[12] On 18 April 2001, the ACE satellite recorded a sudden increase of the SW dynamic pressure from ~ 1 to

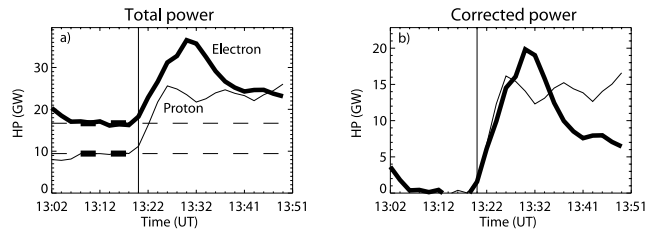


Figure 1. Method used to separate the contribution of the shock aurora from other auroral signal or residual background contamination. Figure 1a represents the time evolution of the precipitated power due to electrons (thick line) and protons (thin line). The correction is performed by subtracting the average of the signal during the minutes preceding the shock. The resulting time variation is shown in Figure 1b.

~ 10 nPa at 0004 UT (Figure 2). This enhancement was caused by a sharp variation of both the SW density (from 5 cm^{-3} to 25 cm^{-3}) and the SW velocity (from 350 km s^{-1} to 500 km s^{-1}). A sharp increase of the magnetic field magnitude was simultaneously observed (from 5 nT to more than 20 nT) while the B_z component dramatically decreased from ~ -2 nT to ~ -20 nT. This shock took place following a long period (over 24 hours) of slightly negative B_z . Figure 3 shows that the first effect on auroral precipitation was observed 43 min later (0047 UT) in the prenoon region for electrons and in the postnoon region for the protons. During the 10 min following the shock, the global dynamics is different for electron and proton precipitation. Proton precipitation quickly propagates anticlockwise to the night-side sector. The morning sector remains undisturbed during the entire event and the postmidnight region is activated ~ 6 min after the first dayside enhancement. The electron precipitation enhancement propagates mainly through the morning sector immediately after the shock and manifests itself in the afternoon sector 2 min later. The speed of propagation of the proton disturbance to the night sector appears faster than electron. This is readily seen 2 min after the first dayside enhancement when proton activity has already reached the 2100 MLT sector ($\Delta \text{MLT} \approx 9$), whereas the electron emission is still in the morning sector ($\Delta \text{MLT} \approx 6$). The midnight region remains quiet during the first 8 min both for proton and electron precipitation. Twelve minutes after the shock, auroral activity covers mainly the premidnight sector both for electron and protons. This auroral brightening is mainly due to the northward motion of the poleward boundary of the precipitation region.

[13] Figure 4 presents the time evolution of the global precipitated hemispheric power (HP) (Figure 4a) and the power observed in different MLT sectors (sector power, SP) (Figures 4b–4f) for both electrons and protons. One point is obtained every 2 min and the curves are smoothed over three data points. The HP reaches a value of ~ 60 GW 20 min after the arrival of the shock (~ 45 GW due to electron and ~ 15 GW due to proton precipitation). The noon sector is centered on the local noon and extends from 1000 to 1400 MLT. This region first brightens immediately following the shock arrival as shown by the rapid rise of the SP (Figure 4b). The power starts increasing ~ 2 min before 0047 UT on Figure 4 due to the smoothing applied on these

curves. Taking this effect in account, the precipitated power reaches a peak of 6 GW 2 min after the shock. The variation of activity in this sector is sharper but more short-lived than in other MLT regions. In the afternoon sector (1400–1700 MLT) (Figure 4c) and the morning sector (0700–1000 MLT) (Figure 4d) a weak increase of the precipitation (less than 1 GW) is observed a few minutes before the shock. After the arrival of the shock, the activity enhancement is quasi-simultaneous in the two sectors for protons, but the precipitation is smaller in the morning sector. The most conspicuous asymmetry is seen in the electron precip-

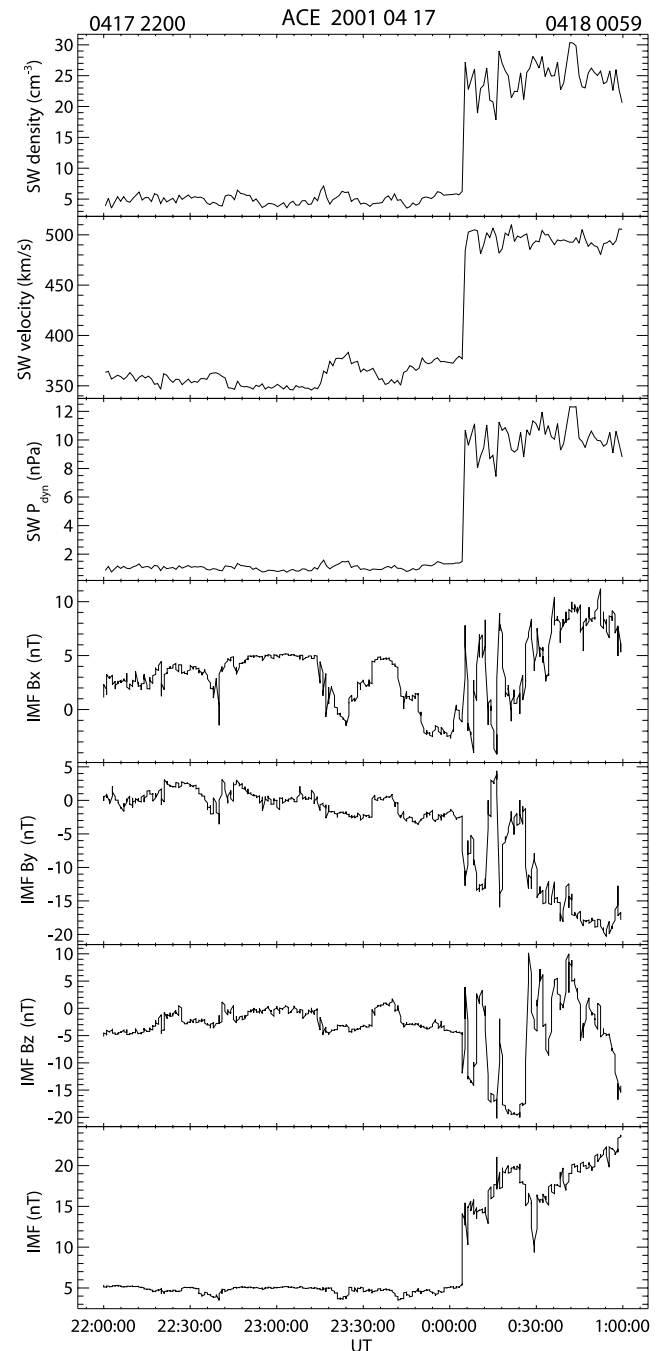


Figure 2. Solar Wind (SW) and Interplanetary Magnetic Field (IMF) data recorded by the ACE satellite between 17 April 2001 at 2200 UT and 18 April at 0100 UT.

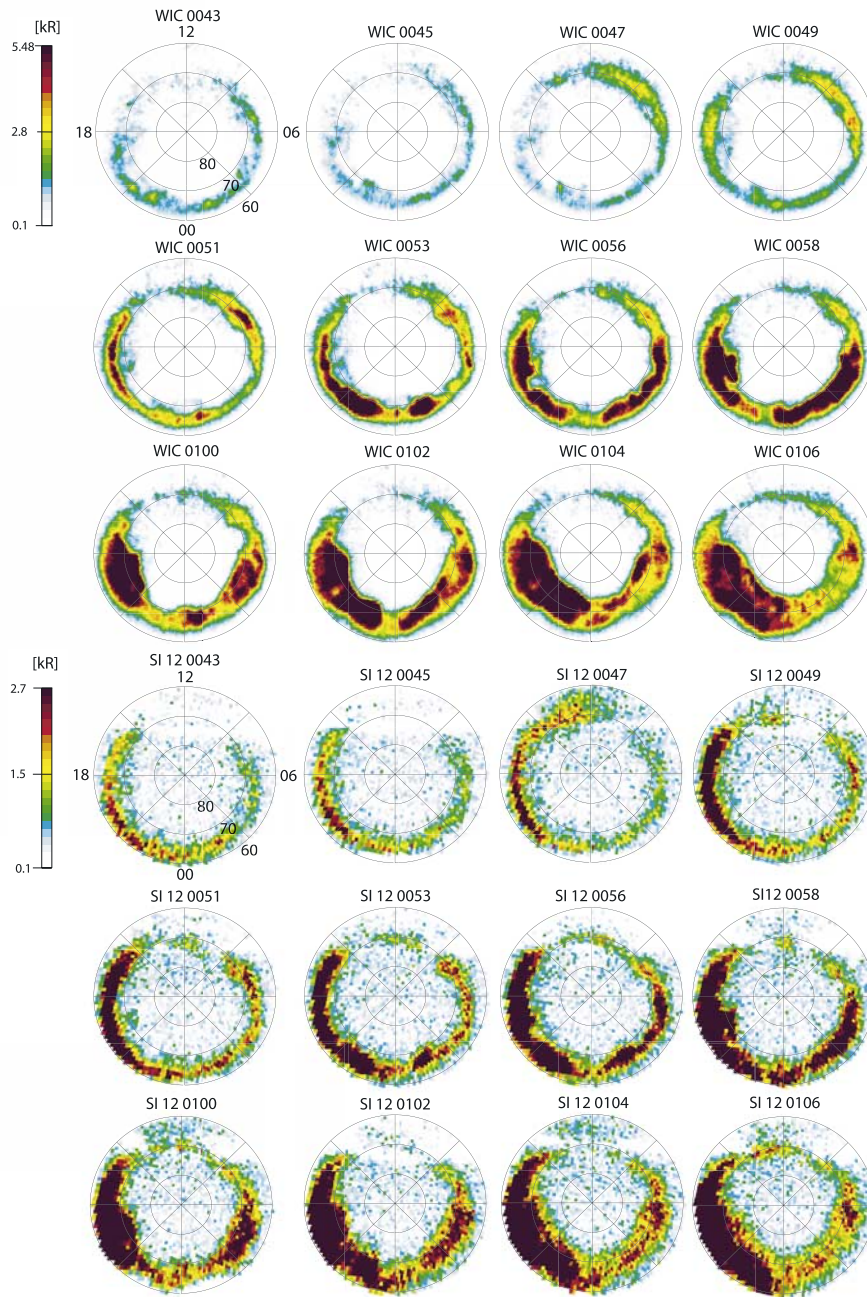


Figure 3. Sequence of WIC (top) and SI12 (bottom) images from the northern hemisphere displayed on a geomagnetic grid with local noon at the top of each image. The data were obtained during southward B_z conditions on 18 April 2001 between 0043 and 0106 UT. The WIC signal is mainly due to electron precipitation and the SI12 instrument is solely sensitive to proton aurora.

itation evolution. This evolution in the afternoon sector is gradual and remains weak (+1 GW in 8 min), whereas it is three times more important in the morning sector (+3 GW in 8 min). Almost 6 min after the shock-induced precipitation is initiated in the noon sector, the level of activity grows in both nightside sectors (Figures 4e–4f). Asymmetry about the noon-midnight axis is clearly observed. The total precipitated power is also quite different with ~ 40 GW in the premidnight region and ~ 20 GW in the postmidnight

sector. During this event, the relative contribution of protons to the precipitated power on the entire oval is greater than 25% (Figure 4g). The asymmetry observed in the night sector (1900–2300 UT and 0100–0500 UT) is also visible in terms of relative proton contribution with a weaker proton precipitation in the postmidnight region (0100–0500 UT). To separate the effects of the shock from those of a substorm possibly triggered by the shock, the midnight sector is avoided, since most electron and proton substorm

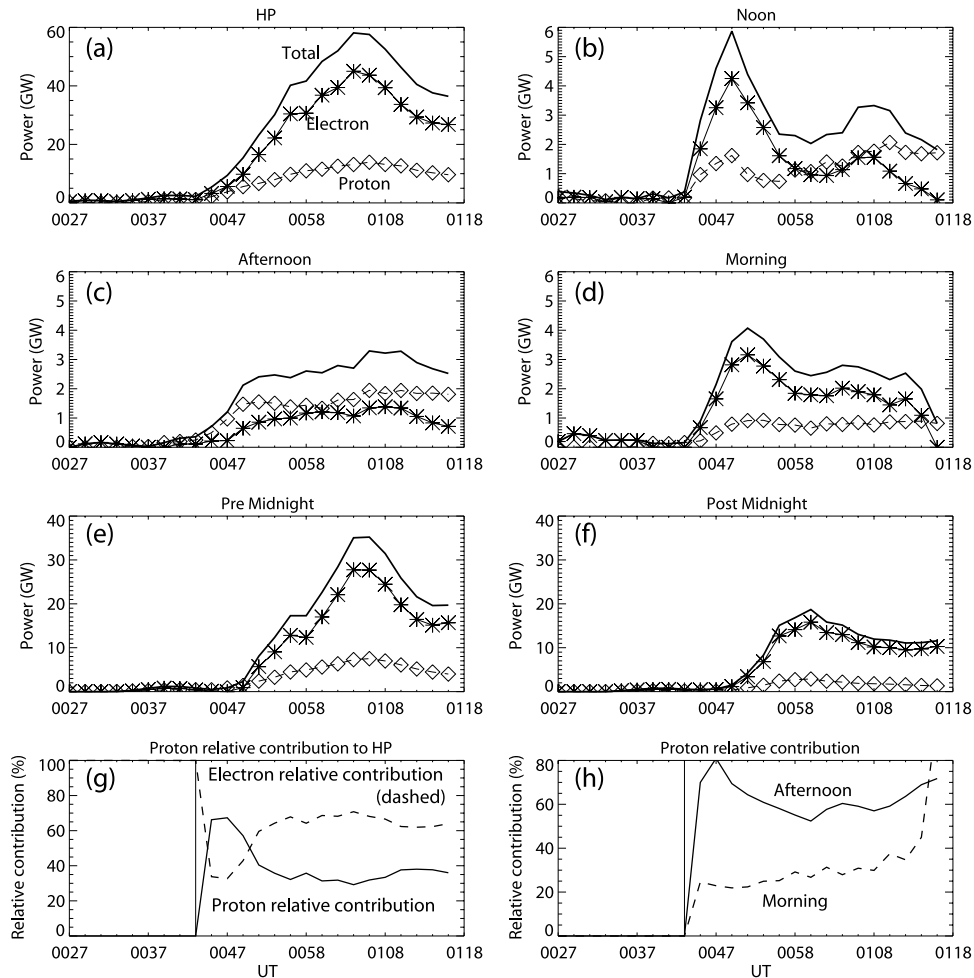


Figure 4. Time evolution of the precipitated power (GW) observed during the 18 April 2001 event (a) in the entire oval and (b) to (f) in different sectors. (b) The noon sector extends from 1000 to 1400 MLT and 50° to 80° MLAT. The (d) morning and (c) afternoon sectors are symmetrically located from 0700 to 1000 MLT and 1400 to 1700 MLT, respectively, with a latitudinal expansion from 60° to 80° MLAT. The nightside region is divided in two sectors, (e) 1900 to 2300 MLT (premidnight) and (f) 0100 to 0500 MLT (postmidnight). As on the dayside, the latitude extends from 60° to 80° MLAT. The vertical scale used for the three dayside sectors is different from that used in the nightside sectors. Stars show the power of the electron precipitation, diamonds indicate the proton power and the solid line represents the total power. The evolution of the proton relative contribution to HP is represented in Figure 4g and the comparison between proton relative contribution in the afternoon and morning sectors is given in Figure 4h.

onsets occur in this region [Liou *et al.*, 2003; Gérard *et al.*, 2004].

3.2. Shock Event of 8 November 2000

[14] On 2 November 2000, ACE measurements show a long period of low dynamic pressure (~ 2 nPa) until 0500 UT and a strong increase to ~ 18 nPa in less than 12 min (Figure 5). This jump of the dynamic pressure is essentially due to an abrupt SW density change (from 7 cm^{-3} to over 50 cm^{-3}), whereas the SW speed remained close to its initial value ($455 \pm 10 \text{ km s}^{-1}$ during the shock). The large dynamical pressure lasted for nearly 30 min until 0530 UT when the solar wind characteristics returned to values close to the period preceding the shock. During these 30 min, the magnitude of the IMF decreased from ~ 17 nT to ~ 5 nT. The B_z component had a large positive value

(15 nT) before the shock and dropped to values close to 0 nT. The B_x and B_y component were essentially unaffected by the pressure pulse. The FUV images showed the first response to the shock in the dayside sector at 0612 UT (Figure 6). The signature is more conspicuous in the proton precipitation observed with the SI12 camera. At 0612 UT, injections occurred mainly in the afternoon region. In the afternoon sector, the proton enhancement is more intense than the electron one. A particular proton feature appeared 2 min later (0614 UT), as was described by Hubert *et al.* [2003]. It consists of a short-lived proton precipitation at very low latitudes (between 50° and 60° MLAT in the 100–1400 MLT sector), that is at the footprint of magnetic field lines crossing the equatorial plane at distances as small as $4\text{--}7 R_E$. This proton flash completely faded out 10 min after it first appeared. The cusp proton signature is visible on the

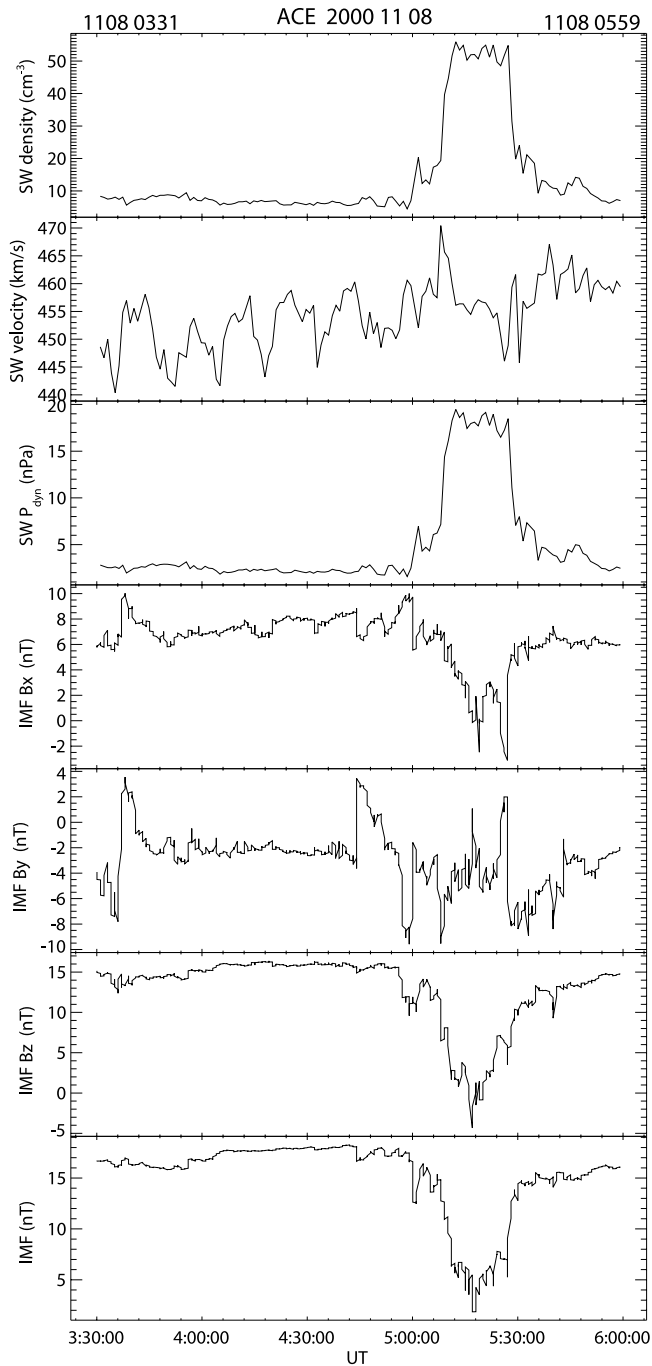


Figure 5. Solar Wind and Interplanetary Magnetic Field recorded by the ACE satellite on 8 November 2000 between 0330 and 0600 UT.

oval at noon. Its aspect and location are in agreement with the description by *Frey et al.* [2002], who showed that the cusp signature on the dayside is confined to a spot inside the main oval during periods of positive B_z . During the fading phase of the proton flash, the activity in the morning and postmidnight sectors was enhanced both for protons and electrons and a transpolar arc developed at local noon as observed with SI12 and WIC.

[15] Figure 7 presents the sector and hemispheric powers from 0539 to 0626 UT. With a peak value around 4 GW,

the total HP is lower than for the negative B_z case described before. As previously, the power plots are smoothed on three points with a box function. The main increase of the HP occurs at 0610 UT but a first increase is observed between 0602 and 0608 UT, probably connected to the rise of dynamic pressure observed by ACE between 0500 and 0510 UT. The maximum HP is reached approximately 10 min later owing to the arrival of the main dynamic pressure pulse. The auroral power variation is fastest in the noon sector (1000–1400 MLT). In the morning sector (0700–1000 MLT), the peak is reached after 4 min and this value remains quasi-constant until ~ 2 min before the relaxation period. In the afternoon sector (1400–1700 MLT), the rise time is very similar to the noon sector but the maximum power is only half and the relaxation phase is smoother. A different behavior is observed in the morning sector with a rise time of 10 min. In the nightside sectors, clear asymmetry about the noon-midnight axis is again observed. In the premidnight region (1900–2300 MLT), the power increase is low and long lasting, while in the postmidnight sector it reaches a plateau ~ 10 min after the arrival of the main shock. The initial increase is observed in the afternoon sector and immediately after in the noon MLT sector. The nightside enhancement occurs a few minutes later in the postmidnight regions. The relative proton contribution to the power in the entire oval is higher than in the previous event with a contribution close to 50% (Figures 7a and 7g). The difference between the proton contribution to the power in the morning and afternoon regions is lower than in the 28 April 2001 event (Figure 7h), but in the nightside region the proton contribution is large with values greater than 50% whereas dayside values are typically around 30%.

3.3. Summary

[16] The two cases described before occurred during situations characterized by a different orientation of the IMF B_z component during a period extending from 90 min before the shock to 10 min after. They show both differences and similarities. In both cases the initial response is observed on the dayside, followed by a propagation of enhanced precipitation to the nightside with a larger amount of precipitated power on the nightside than the dayside. Asymmetries with respect to the noon-midnight axis are also observed in both cases. The main difference is a larger precipitated power observed during the negative B_z event at each MLT with a dramatic increase of the activity on the nightside. This sensitivity to the sign of B_z in the midnight sector was visible in Figure 5c presented by *Liou et al.* [1998]. In the noon region, the precipitated power for negative B_z is almost three times larger than for positive B_z . This tendency is also observed in the morning and afternoon sectors. The maximum precipitated power on the nightside is dramatically higher for negative B_z than in the positive B_z context. However, it is not clear that this higher activity is a substorm triggered by the shock. Indeed, in this case, no onset can be identified and no brightness surge from local midnight is observed eastward or westward. This criterion using the morphological evolution of activity seems to be better to identify substorms than magnetic bays, since the majority of the magnetic bays found by *Liou et al.* [2003] were not accompanied by auroral break-

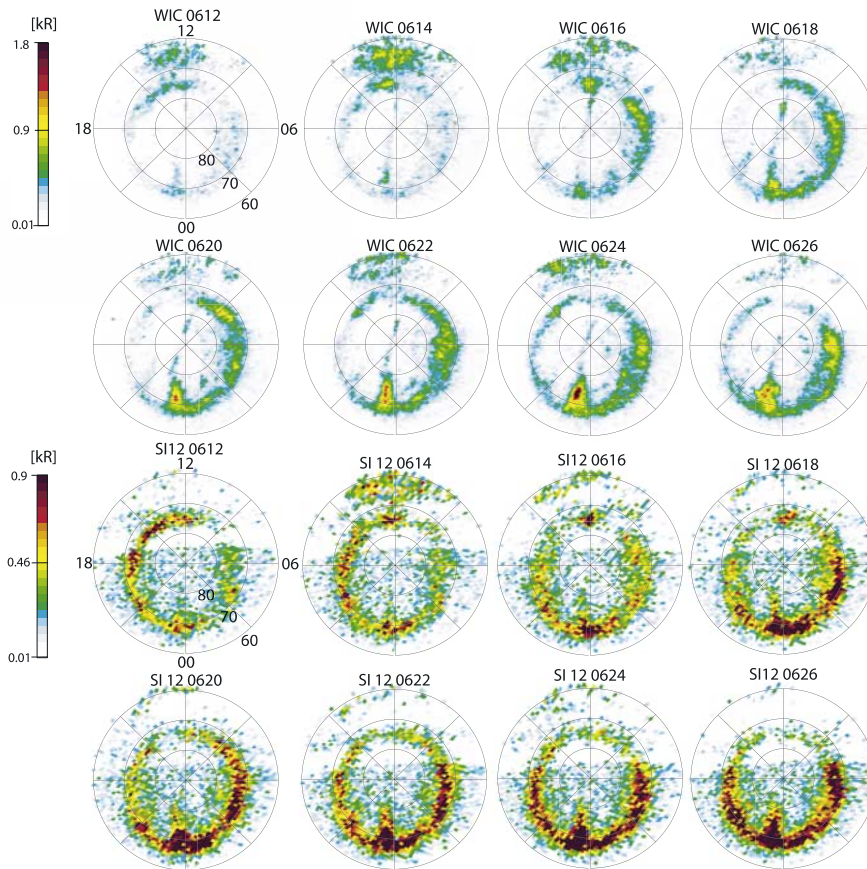


Figure 6. Sequence of WIC (top) and SI12 (bottom) images of the northern hemisphere displayed on a geomagnetic grid with local noon at the top of each image. The data were obtained during positive B_z conditions on 8 November 2000 between 0612 and 0626 UT.

ups. After the shock, the relative proton contribution to the total power appears larger for the case occurring during the northward B_z period. This global behavior is mainly due to precipitation observed on the nightside sector where the evolution of the precipitated power due to electrons is particularly weak. During southward B_z events, an asymmetry between the morning and the afternoon sectors is observed in the proton relative contribution to the precipitated power.

4. Statistical Study

[17] As mentioned before, the shock events used for this study were selected based on ACE and FUV observations. They meet criteria of availability of data before and after the shock, field of view coverage of the regions of interest, and induced auroral brightness in comparison with other sources of FUV signal. These events were thus selected independently of the existence of a shock-induced substorm. The intensity of the response to the shock may be very different from one case to another but the calculated power for each case is used without any further normalization applied. The list of cases meeting these conditions is given in Table 1.

[18] It is seen that in all 14 cases, the sign of B_z averaged over 30 min prior to the shock did not change during the following 10 min period. The two negative Dst variations,

occurring during negative B_z periods, indicate that the negative variation of the Dst index caused by the induced substorm is more important than the Dst increase due to the compression.

[19] The statistical analysis of this study is presented in two different sections. We first describe the time evolution of the power injected in the entire auroral oval and in different MLT sectors. In a second section, we investigate the correlation of the auroral activity with the solar wind and the IMF parameters.

4.1. Time Evolution

[20] To describe the mean time evolution of auroral activity in a given sector, we first calculate the value of the precipitated power in this sector as a function of time for each individual shock aurora with a resolution of 2 min. In order to isolate the increase of power due to the arrival of the shock, the mean value of the power over the 16 min (eight FUV images) preceding the shock is subtracted from each individual case as explained before. For the epoch analysis, in order to synchronize the time of onset of all cases in the noon sector, a time shift is determined for each case and applied to all sectors. No time stretching is applied to the curves in order to keep the real rise time of the shock-induced activity. The curves are then averaged and smoothed on three consecutive points. The proton contri-

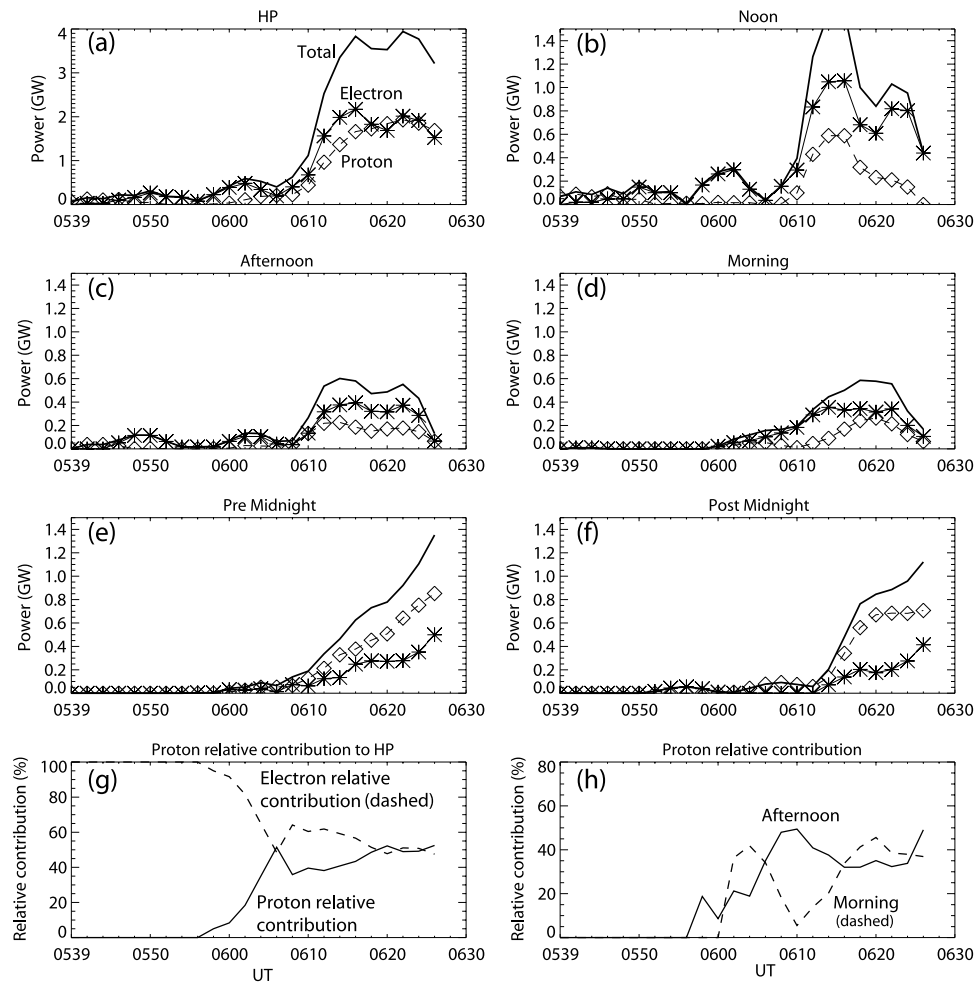


Figure 7. Same as Figure 4 for powers observed on 8 November 2000.

bution to the total power during substorms is generally under 20%.

4.1.1. Hemispheric Powers

[21] Considering all cases independently of the direction of B_z , Figure 8g shows that at the global scale, the relative contribution of proton precipitation to the total power remains remarkably close to 20% with a small difference

at the beginning of the activity surge. Unexpectedly, this percentage varies if the sample of events is divided according to the sign of B_z . The time evolution of the HP for positive B_z cases presented in Figures 9a and 9g shows a proton contribution greater than 30% 10 min after the activity onset. For events occurring during a period of negative B_z (Figure 10a), both electron and proton activity

Table 1. List of the Cases Used in This Study^a

| Year/Day, mm/dd | Time of the Shock, UT | Sign of B_z Before the Shock, 30 min | Sign of B_z After the Shock, 10 min | Δ Dst Index |
|------------------|-----------------------|--|---------------------------------------|--------------------|
| 2000/208 (07/26) | 1859 | <0 | <0 | +4 |
| 2000/261 (09/17) | 0043 | <0 | <0 | - |
| 2000/277 (10/03) | 0056 | <0 | <0 | -10 |
| 2000/309 (11/04) | 0224 | >0 | >0 | +21 |
| 2000/311 (11/06) | 0949 | <0 (with 8 min of $B_z > 0$) | <0 | +10 |
| 2000/313 (11/08) | 0558 | >0 | >0 (with 4 min of $B_z < 0$) | - |
| 2000/342 (12/07) | 0721 | >0 (with 8 min of $B_z < 0$) | >0 | - |
| 2001/010 (01/10) | 1609 | <0 | <0 | +4 |
| 2001/018 (01/18) | 0950 | Oscillations around $B_z = 0$ | >0 | - |
| 2001/108 (04/18) | 0047 | <0 | <0 | -2 |
| 2001/118 (04/28) | 0458 | >0 | >0 | +6 |
| 2001/298 (10/25) | 0853 | >0 | >0 | +7 |
| 2001/364 (12/30) | 2011 | >0 | >0 | +27 |
| 2002/077 (03/18) | 1322 | Oscillations around $B_z = 0$ | <0 | +29 |

^aFor each case, the dominant sign of B_z before and after the shock is mentioned as well as the variation of the Dst index between the 3 hours preceding the shock and the hour following the perturbation. Dst values are not mentioned in cases when sudden impulse events were recorded by less than five low-latitude stations (World Data Center for Geomagnetism, WDCG).

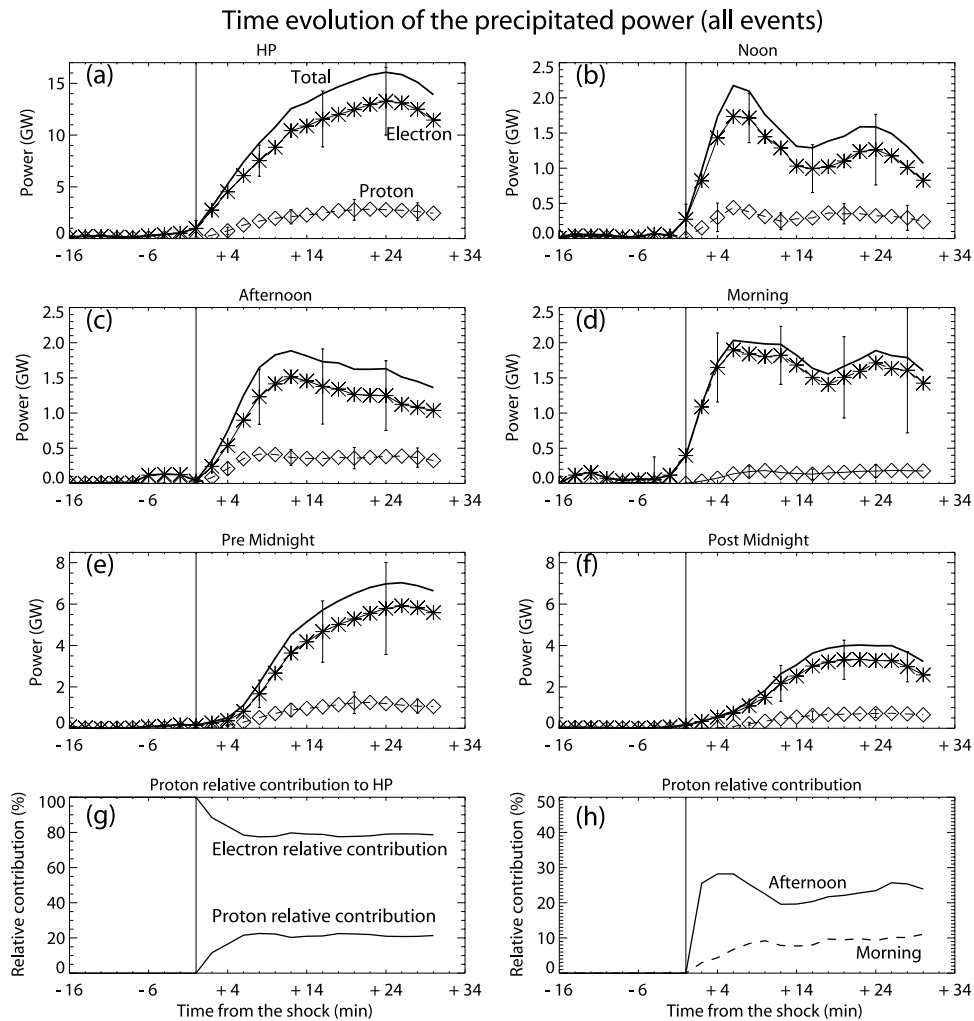


Figure 8. Epoch analysis of the power precipitated (a) in the entire oval and in different sectors as follows: (b) noon (1000–1400 MLT, 50° – 80° MLAT), (c) afternoon (1400–1700 MLT, 60° – 80° MLAT), (d) morning (0700–1000 MLT, 60° – 80° MLAT), (e) premidnight (1900–2300 MLT, 60° – 80° MLAT), (f) postmidnight (0100–0500 MLT, 60° – 80° MLAT). For better readability, only one error bar is plotted every 4 points. The total injected power is represented by the solid line and the evolution of electron and proton contributions is given by the stars and the diamonds curves, respectively. The vertical scale used for the three dayside sectors is different from that used in the nightside sectors. The mean evolution of the proton relative contribution to HP is represented in Figure 8g and the comparison between proton relative contribution in the afternoon and morning sectors is shown in Figure 8h.

are enhanced with respect to the Figure 8a but differently for electrons and protons. The increase is around 14% for protons and $\sim 65\%$ for electrons. During negative B_z events, the relative proton contribution to the total power is $\sim 15\%$ (Figure 10g), i.e., more than two times smaller than for positive B_z events. The rise time of the HP is 15–20 min, independent of the sign of B_z and the mean maximum of HP is ~ 15 GW, a lower value than during isolated substorms events, which typically peak between 40 and 100 GW [Lummerzheim *et al.*, 1997; Hubert *et al.*, 2002; Østgaard *et al.*, 2002].

4.1.2. Sectorial Powers

[22] The time evolution of the auroral power averaged on all cases is shown for each sector in Figures 8b–8f. The power in the noon sector (Figure 8b) shows a sharp rise (a factor of 6 in 6 min) with a proton contribution to the total

power of this sector close to 20%. Following the peak, the power drops faster than in any other sector. The time delay between the initial enhancement and the plateau is ~ 14 min. Different characteristics are observed in the morning and afternoon sectors, symmetrically located with respect to the noon-midnight axis. The proton contribution is more important both in relative and absolute values in the afternoon sector (Figure 8c) than in the morning sector (Figures 8d and 8h). The rise time of the proton power in the afternoon region is comparable to the noon region. By contrast, the afternoon sector is different from the noon region with a lower and smoother electron precipitation. The relative proton contribution to the power in the two night sectors is comparable with a value of $\sim 20\%$. The power reached in the premidnight region is ~ 7 GW compared to ~ 4.5 GW in the postmidnight sector. They

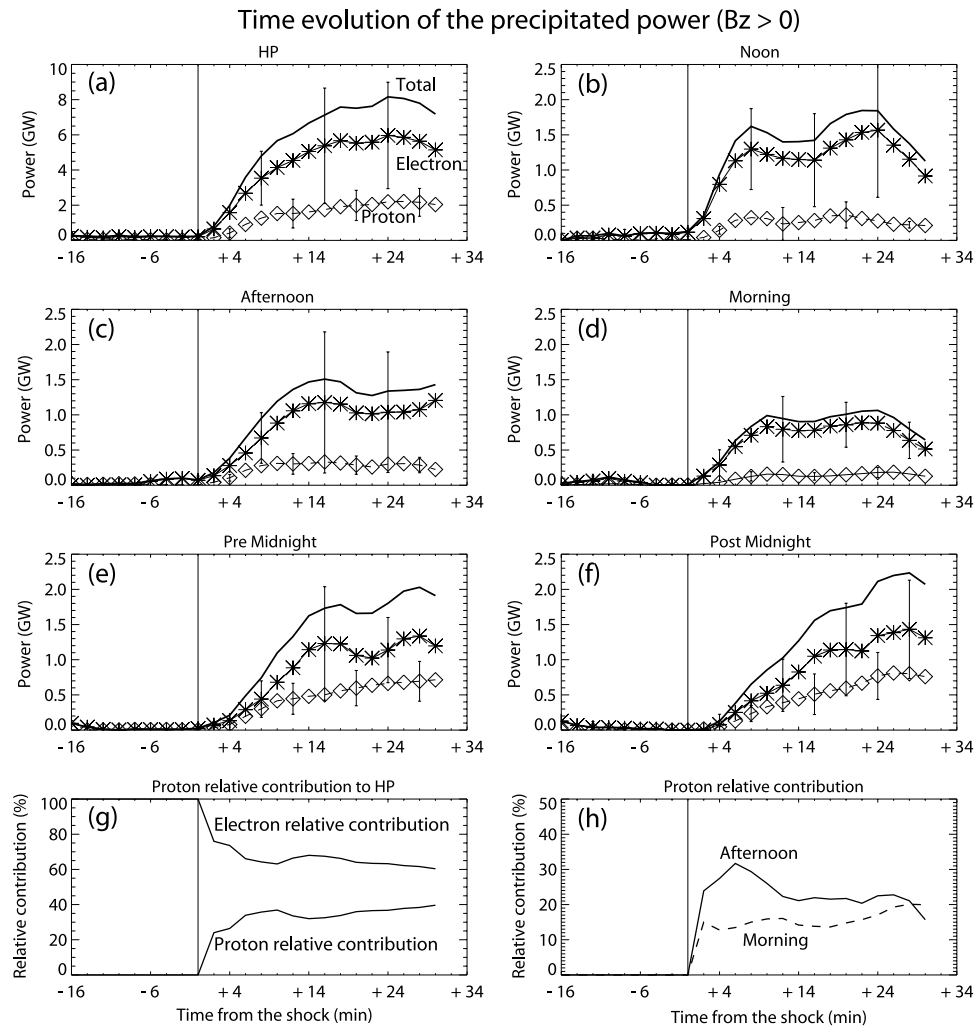


Figure 9. Same as Figure 8 for cases occurring during periods of northward B_z .

both exceed the values found in other sectors. The rise time, common to electrons and protons, is between 15 and 20 min.

[23] The time evolution of the SP is plotted in Figures 9b–9h and 10b–10h separately for cases characterized by northward and southward B_z component carried by the shock plasma, respectively. For cases of positive B_z (Figure 9), the relative proton contribution to the precipitated power is $\sim 25\%$ in the noon region (Figure 9b), which is very similar to the contribution in the afternoon sector (Figures 9c and 9h). This fraction is lower in the morning region with observed values around 15% (Figures 9d and 9h), which presents the lowest relative contribution of the entire oval. In terms of absolute values, the proton power is ~ 0.32 GW in the afternoon sector (Figure 9c) and ~ 0.18 GW in the morning sector (Figure 9d), whereas the power due to electrons is found around 1.2 GW and ~ 0.8 GW, respectively. In the night sectors (Figures 9e and 9f), the relative proton contribution is clearly higher than 20% with a symmetrical distribution around the noon-midnight axis. Over the entire oval, protons contribute for more than 30% of the total power when B_z is positive (Figure 9g). For cases of negative B_z (Figure 10), the relative proton contribution in the noon (Figure 10b) and

afternoon sectors (Figures 10c and 10h) is almost the same as for positive B_z events ($\sim 25\%$) but this value clearly decreases in the morning region (5–10%) (Figures 10d and 10h). The absolute proton power is 0.54 GW in the afternoon sector and 0.18 GW in the morning region. The electron contribution to the power in the dayside is larger than for positive B_z , with values around 2 GW in the afternoon region and 3.2 GW in the morning. In the night sectors (Figures 10e and 10f), the relative proton contribution is lower than 20% and is asymmetrically distributed around the noon-midnight axis. The highest power is found in the premidnight sector with ~ 10 GW due to electrons and ~ 1 GW due to protons against ~ 5 GW and 0.8 GW respectively in the postmidnight region. The relative proton contribution on the entire oval is $\sim 15\%$ (Figure 10g) which is significantly lower than for positive B_z events.

[24] In summary, this epoch analysis presents similarities between events occurring during positive and negative B_z conditions. The power associated with proton precipitation is more important in the afternoon region than in the morning for both signs of B_z . The electron precipitation is also observed to be weaker in the afternoon than in the noon sector, independently of the sign of B_z . It also appears that behavior observed in the afternoon region is independent of

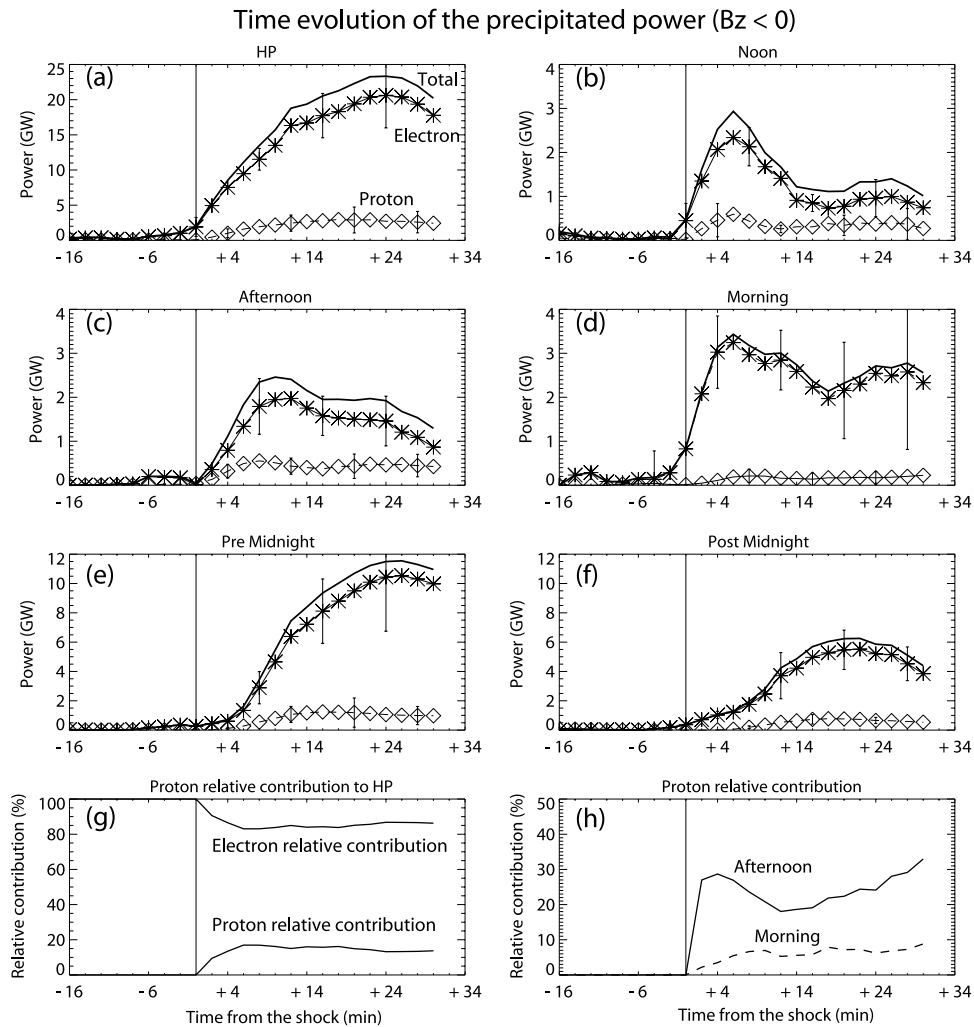


Figure 10. Same as Figure 8 for cases occurring during periods of southward B_z .

the sign of B_z . Differences due to the sign of B_z are also enhanced. It appears that the relative proton contribution to the power is actually smaller in almost all individual sectors for cases of negative B_z but quite similar in the afternoon region. This is a consequence of the large electron contribution observed during southward B_z cases. The sign of the B_z component also exerts a greater control on auroral activity on the nightside than on the dayside. Indeed, the maximum power in the noon sector is about 3.2 GW for negative B_z and ~ 1.6 GW for positive B_z . The difference is larger in the premidnight region with a maximum of ~ 12 GW reached 20 min after the onset for $B_z < 0$, compared with a peak value less than 2.5 GW for cases with $B_z > 0$.

[25] In terms of propagation around the oval, proton precipitation is more important in the noon-dusk-midnight half of the oval than in the other half of the oval. Both for northward and southward B_z , the time evolution of proton activity is very similar in the noon and afternoon regions and the rise starts simultaneously in the two sectors. Absolute proton fluxes injected in morning sectors are similar for all directions of B_z , whereas the relative proton contribution to the total power is more important when B_z is positive. The largest proton power occurs on the nightside. A higher injected power in the premidnight sectors is

observed when B_z is oriented southward whereas the distribution is more symmetric during northward B_z events. Electron precipitation appears different. During southward B_z events, it is more active in the morning sector (maximum at ~ 3.5 GW) than in the afternoon (~ 2 GW). On the nightside, as for proton activity, the maximum is reached in the premidnight sector. When B_z is oriented northward, the power due to electron is similar on each side of the noon-midnight axis both for the dayside and the nightside region of the oval. The time delay between the peaks in the noon and the night sector is ~ 18 min but the time elapsed between the beginning of the activity rise in the noon and nightside sectors is only ~ 4 min.

4.2. Correlation Between Auroral Activity and SW and IMF Parameters

[26] Several authors [Burch, 1972; Zhou and Tsurutani, 2001; Liou et al., 2002] studied the influence of solar wind shocks as triggers of auroral activity in the nightside sector. They found a good correlation between nightside auroral activity generated by shocks and IMF parameters averaged on the 90 min preceding the shock. They interpreted this integration period in terms of a loading mechanism of the plasma sheet. The study developed in this section is

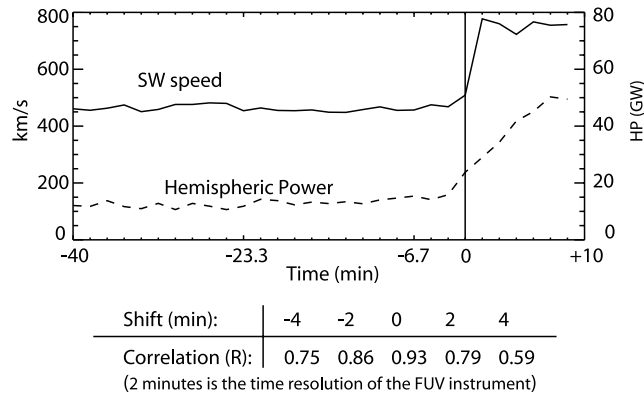


Figure 11. Example of cross-correlation method applied to the 28 April 2001 event. The table represents the Pearson coefficient obtained for the correlation calculated for each 2 minuteshift. This example shows that the best correlation between the SW speed (propagated to the front of the magnetosphere) and the HP is obtained when no time shift is applied.

fundamentally different than the effect of the well-known preconditioning mechanism. It concerns the impact on the precipitated power of the characteristics of SW and IMF carried by the shock. In spite of the low number of events, the relationships between SW or IMF parameters and the additional auroral power triggered by the shock are investigated. To isolate the effect of SW and IMF parameters, a correlation study is presented using the Fisher transform. This method applies to large enough samples and, consequently, results presented in the following paragraphs only provide a trend that might be supported by a larger data set. To calculate the power added by the shock, as before, the mean value of the power during the 16 min prior to the shock is subtracted from the total power. The method is first described and results are then presented.

[27] The pertinence of the time period chosen for this correlation is assessed using a cross-correlation method. We cross-correlate both the SW or IMF evolution (time-shifted based on the distance between the ACE satellite and the front of the magnetosphere) and the time evolution of the injected power in a given sector. An example is presented in Figure 11. Curves represent the evolution of SW speed

(shifted by the calculated time delay) and the HP for the 28 April 2001 event. Time $t = 0$ corresponds to the arrival of the shock on the front of the magnetosphere as measured from the WIC signal. Figure 11b gives the cross-correlation between the two vectors. The shift giving the best correlation is interpreted as the response time of the magnetosphere to the rapid SW and IMF changes. Positive values of the shift imply a response time to SW and IMF changes greater than 2 min (which is the time resolution of the FUV instrument). A null value of the shift implies a response time less than 2 min and a negative value would suggest an unrealistic situation where the auroral response precedes the SW or IMF perturbation. In this example, it is found that a null value of the time shift gives the best correlation. The distribution functions of the shifts are represented in Figures 12a and 12b for the correlation with the solar wind speed v and the magnitude of the magnetic field B , respectively. As mentioned before, negative values are unphysical and are likely associated with errors in the determination of the propagation time of the shock from the ACE satellite to the front of the magnetosphere. Errors on this propagation time induce a shift of the horizontal axis and a widening of the curves in Figures 12a and 12b. If the distribution of these errors is normal, information about the time delay between the SW and IMF variations and their auroral responses is contained in the asymmetry of these curves. The centers of the Gaussian fits applied on these curves (if the peaks are withdrawn) are separate of the peaks by ~ 5 min. This value provides an idea on a mean delay separating a SW-IMF variation from the auroral response. Since the FWHM of these Gaussian curves is lower than 5 min, the integration time used on SW-IMF values and precipitated powers for the correlation study developed in the following paragraphs is 10 min. This integration time allows to avoid problems due to uncertainties on the propagation time of SW from ACE to the front of the magnetosphere and to be sure that the auroral reaction to the shock is taken in account.

[28] The Pearson correlation coefficient is calculated from the formula:

$$R = \frac{n(\Sigma XY) - (\Sigma X)(\Sigma Y)}{\sqrt{[n\Sigma X^2 - (\Sigma X)^2][n\Sigma Y^2 - (\Sigma Y)^2]}}, \quad (1)$$

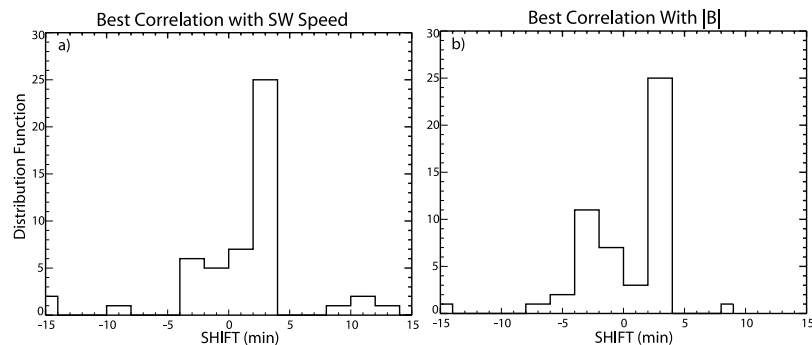


Figure 12. Distribution function of time shifts applied to obtain the best correlation of the power precipitated both in the day and night sectors with (a) the solar wind speed and (b) the magnitude of the magnetic field.

Table 2. Linear Correlation Coefficients Between Auroral Power and Solar Wind Parameters^a

| | $B_z < 0$ | | | | | | $B_z > 0$ | | | | | |
|-------------------------|-------------|-------|------|-------------|-------------|-------------|-------------|-------------|-------------|------------|-------------|-------------|
| | Electrons | | | Protons | | | Electrons | | | Protons | | |
| | Day | Night | HP | Day | Night | HP | Day | Night | HP | Day | Night | HP |
| B | <u>0.7</u> | 0.56 | 0.66 | <u>0.9</u> | <u>0.68</u> | <u>0.79</u> | <u>0.75</u> | <u>0.81</u> | <u>0.8</u> | 0.54 | <u>0.96</u> | <u>0.81</u> |
| $\Delta\rho$ | <u>0.37</u> | 0.39 | 0.41 | <u>0.37</u> | <u>0.25</u> | <u>0.3</u> | -0.24 | -0.25 | -0.25 | -0.33 | -0.28 | -0.32 |
| ΔP_{dyn} | 0.47 | 0.49 | 0.52 | 0.55 | 0.43 | 0.49 | 0.14 | 0.06 | 0.12 | 0.07 | 0.06 | 0.09 |
| v | 0.43 | 0.47 | 0.49 | <u>0.82</u> | <u>0.83</u> | <u>0.84</u> | <u>0.86</u> | <u>0.7</u> | <u>0.84</u> | <u>0.9</u> | <u>0.78</u> | <u>0.9</u> |

^aUnderlined numbers correspond to the best correlations (confidence level above 90%).

where Y is the calculated increase of power due to the shock in a defined sector, X is the SW or IMF parameter to be correlated, and n is the number of elements of the X and Y vectors. The Fisher transform is applied using the relation

$$Z = \frac{1}{2} \ln\left(\frac{1+R}{1-R}\right). \quad (2)$$

For a fixed value of the confidence parameter α , $u_{1-\frac{\alpha}{2}}$ is calculated from the relation

$$F\left(u_{1-\frac{\alpha}{2}}\right) = 1 - \frac{\alpha}{2}, \quad (3)$$

where F is the Gaussian distribution. The correlation between X and Y has a level of confidence $(1 - \alpha) \times 100$ if the relation

$$-\frac{u_{1-\frac{\alpha}{2}}}{\sqrt{n-3}} \leq Z \leq \frac{u_{1-\frac{\alpha}{2}}}{\sqrt{n-3}} \quad (4)$$

is not verified and the correlation is below this confidence level if this relation is satisfied. This method provides a way to determine whether two quantities are correlated, taking in account the size of the sample. The size of the sample is linked to the confidence level. Indeed, Z approaches a normal distribution for an increasing size of the sample. Above a critical size (~ 10 events), Z may be approximated by a Gaussian distribution and the confidence level may be defined as above [Press *et al.*, 1989]. In this study, a value of $\alpha = 0.1$ is used, corresponding to a correlation at a confidence level of 90%. The correlation study considers the link between auroral power (for the day, the night, and the full oval) averaged over the 10 min following the shock and the magnetic field intensity (B), plasma density carried by the shock (ρ), dynamic pressure (P_{dyn}), and the SW bulk speed (v) averaged over the same period. The night sector is included in this study not only to consider possible shock-induced substorms but mainly to provide a global view of shock-induced effects. Correlations are calculated separately for cases with positive and negative B_z component. Table 2 compiles the Pearson coefficient (R) matrix for all parameters. These correlation coefficients are obtained for a sample of six events occurring during a period of negative B_z and seven events occurring when B_z is positive. The following example illustrates the method used in Table 2 for the correlation between HP due to electron precipitation and the magnitude of the magnetic field during negative B_z events. Vectors are

$$B = (9.1, 4.24, 8.45, 5.81, 15, 13.26)(\text{nT}) \quad (5)$$

and

$$HP_e = (20.9, 14, 7.09, 2, 21.3, 19.5)(\text{GW}). \quad (6)$$

From equation (1), $R = 0.66$ for this data set of six events what corresponds to a $Z = 0.786$ (equation (2)). Equation (4) gives $u_{1-\frac{\alpha}{2}} < Z$, $\sqrt{n-3}$, i.e., $u_{1-\frac{\alpha}{2}} < 1.36$. Using this value and equation (3), we find $F(u_{1-\frac{\alpha}{2}}) = F(1.36) = 0.91$, implying a value of $\alpha = 0.17$ and consequently a confidence level of 83%. For a set of six events, a correlation coefficient of 0.66 implies thus a confidence level lower than 90%. This result can also be obtained by the reverse method:

$$\alpha = 0.1 \quad (7)$$

$$\Rightarrow F\left(u_{1-\frac{\alpha}{2}}\right) = 0.95 \quad (8)$$

$$\Rightarrow u_{1-\frac{\alpha}{2}} = 1.64 \quad (9)$$

$$\Rightarrow Z > 0.95 \quad (10)$$

$$\Rightarrow R > 0.73. \quad (11)$$

which shows that a confidence level of at least 90% implies a correlation coefficient higher than 0.73 for a sample of six events (the number of events is used from equation (9) to equation (10)).

[29] As the number of events is low, correlations presented in Table 2 must be understood as qualitative and not quantitative results. However, owing to the relatively large differences observed in the correlation coefficients, this method allows to discriminate parameters influencing or not the power injected during shock events. Moreover, the trends obtained in Table 2 are confirmed in Table 3, which is calculated with a sample of 13 events (a sample size where the Fisher test applies [Press *et al.*, 1989]). Numbers underlined in Table 2 correspond to the most significant correlations (confidence level over 90%). For southward B_z , the correlation study does not include the 6 November 2000 case. This event was atypical and its inclusion would significantly alter the conclusions on the statistical behavior of the shock-induced aurora occurring in a negative B_z context. The shock that triggered this event reached the magnetosphere with the highest speed value observed in the set of events under study (~ 600 km/s). As it will be described later, the trend shown by other events is an increase of the injected power with the speed of the shock but this event actually appears as one of the less active shock-

induced aurora. This may be due to the saturation effect described by *Siscoe et al.* [2002], which takes place during southward B_z context for high solar wind electric field. In addition to a high speed, this event was characterized by a very low solar wind plasma density giving only a low amplitude pressure pulse (from less than 1 nPa to ~ 3 nPa). This particular behavior is illustrated in Figure 13.

[30] Table 2 suggests that the precipitated power is not correlated with the solar wind density variation. This lack of correlation is noted both for electrons and protons and is more pronounced for positive B_z events even if the highest correlation coefficient obtain for negative B_z is still low (0.41). It is illustrated by Figure 14 for protons and electrons on the dayside and nightside and the entire oval for northward B_z events. The dynamic pressure P_{dyn} variation appears loosely correlated with the observed power for cases with $B_z < 0$ and is not correlated at all for cases with $B_z > 0$. Correlations obtained for electron and proton precipitations are comparable for both signs of B_z . The sudden P_{dyn} increase acts as a switch triggering auroral activity induced by the shock. However, the actual value of the P_{dyn} jump does not appear to control the intensity of the shock-induced precipitation even though a variation of P_{dyn} is needed to trigger aurora. Even if it is weak, the highest sensitivity to P_{dyn} variations occurs for protons during negative B_z . It also appears that the P_{dyn} variation is closely linked with the P_{dyn} existing during the 10 min following the shock. This is due to similar P_{dyn} values existing before the shock for all studied events (Figure 15). The standard deviation of P_{dyn} existing before each event is $\sigma = 0.83$ compared to a mean P_{dyn} variation of 6.6 nPa.

[31] The two most significant quantities to describe the shock-induced activity appear to be the IMF intensity (B) and the SW bulk velocity (v), both for events with northward and southward B_z . The dependence of the injected power on the average B value is strong. This relationship is illustrated in three MLT sectors by Figure 16 for proton precipitation during negative B_z events. The highest correlation with B is found in the dayside for events with southward B_z , and in the nightside during cases with positive B_z . In addition, even though the sign of B_z determines the part of the oval that is most influenced by the B value, other regions are also influenced by the intensity of the IMF.

[32] For electron precipitation, the sign of the B_z component carried by the shock seems to have an important effect on the control exerted by the speed of the solar wind. For negative B_z events, the electron precipitation induced by the

Table 3. Linear Correlation Coefficient R Between Proton Auroral Power and Solar Wind Parameters for Events Occurring Both During Periods With Positive and Negative Values of B_z^a

| | Protons | | HP |
|-------------------------|---------|-----------|------|
| | Dayside | Nightside | |
| B | 0.47 | 0.49 | 0.5 |
| $\Delta\rho$ | -0.03 | 0.06 | 0.02 |
| ΔP_{dyn} | 0.27 | 0.28 | 0.29 |
| v | 0.59 | 0.36 | 0.48 |

^aUnderlined numbers correspond to the best correlations (confidence level above 90%).

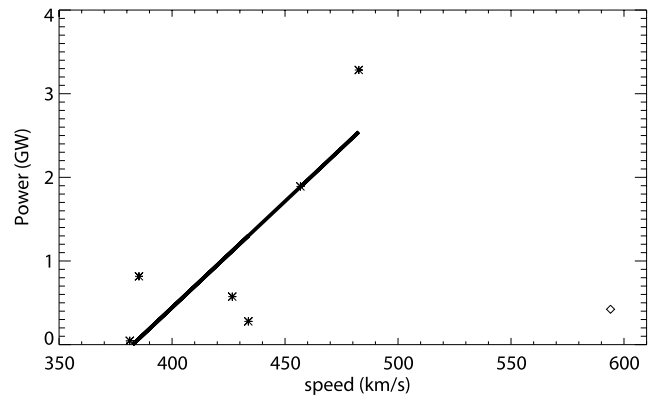


Figure 13. Proton power injected on the dayside (GW) as a function of the solar wind speed (km/s). The line represents the fit to the data when the 6 November 2000 event is removed.

shock appears independent of the solar wind speed, whereas it is a controlling factor during positive B_z events. *Liou et al.* [1998] pointed out the impact of the SW speed during positive B_z events but they also found a dependence when B_z is negative except in the afternoon sector. By contrast, the auroral activity due to protons is linked to the velocity independent of the orientation of B_z independently of the side of the oval considered.

[33] As mentioned above, the size of the sample allows only to isolate trends concerning the influence of SW and IMF parameters on the precipitated power. Using a larger data set considering the entire sample without discrimination based on the sign of B_z , Table 3 also identifies B and v as the parameters influencing the precipitated proton power. This correlation study is only presented for protons since the sign of B_z has an important impact on the intensity of electron precipitation.

5. Discussion

[34] The statistical study of a set of 14 shock-induced aurora may be summarized as follows.

[35] 1. When averaged over all cases, the precipitated power observed in each MLT sector is higher both for electrons and protons during events preceded by a period of southward B_z .

[36] 2. The relative contribution to the HP carried by proton precipitation varies significantly with the sign of B_z . This value is about twice larger for northward B_z than for southward cases.

[37] 3. The relative contribution of proton precipitation to the power injected in the afternoon region is higher than in the morning sector, mainly when B_z is negative. This trend is less important or possibly absent when B_z is positive.

[38] 4. The activity rise is fastest in the noon sector simultaneously for electron and proton precipitation. Electron precipitation in the morning sector and proton in the afternoon region increase at about the same rate.

[39] 5. On the nightside, the MLT distribution is more symmetric during positive B_z events than during negative ones. Negative B_z events present a higher level of electron precipitation in the premidnight area.

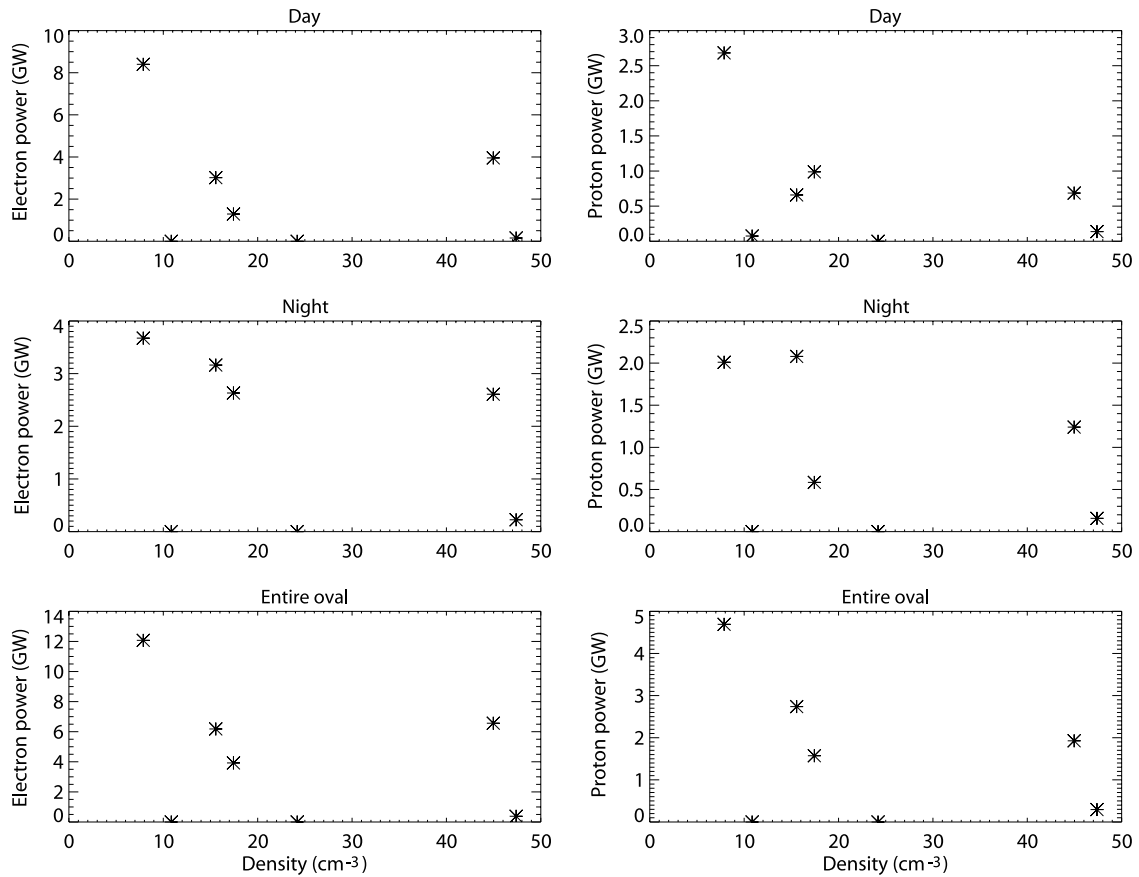


Figure 14. Lack of correlation between the solar wind density variation during the shock and the injected power for electrons (left) and protons (right) for positive B_z cases.

[40] 6. The solar wind density immediately following the shock and the dynamic pressure variation appears weakly correlated or uncorrelated with the power injected during the 10 min following the shock. However, a variation of the dynamic pressure is needed to trigger the auroral activity.

[41] 7. By contrast, the injected power seems linked with B and v values following the shock. These quantities appear as key parameters influencing the intensity of the shock-induced precipitation. Correlation with the magnetic field intensity is higher for the power injected on the dayside when B_z is negative and in the nightside when B_z is positive. Correlation with the solar wind speed is pronounced, except for electron precipitation for negative B_z .

[42] Substorms and shock events present a common dramatic increase of HP due to electron precipitation when B_z is negative. For shock events, this trend is mostly observed on the nightside where the same mechanisms could be called upon for shock and substorm events. The higher hemispheric power associated with southward B_z is likely linked to reconnection processes occurring at the front and in the tail of the magnetosphere. Reconnection at the dayside magnetopause generates a transfer of energy [Tsurutani *et al.*, 2001] and plasma to the magnetosphere while reconnection in the tail triggers explosive plasma injections in the nightside sector, which explain the larger influence of B_z on this region. Field-aligned currents and adiabatic compression mechanisms generate discrete and diffuse aurora in the dayside sector as summarized by

Tsurutani *et al.* [2001] and Zhou *et al.* [2003]. The compression mechanism is consistent with the rapid growth observed in the noon sector (point 4 of our summary), since this sector is the nearest to the front of the perturbed magnetopause. It is also consistent with the similar electron

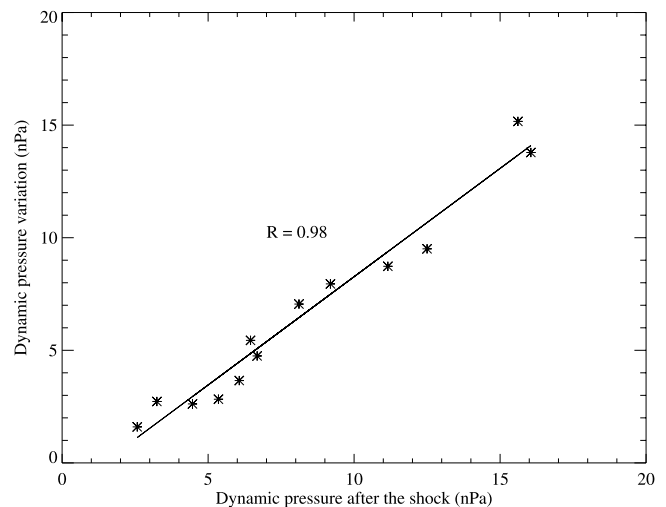


Figure 15. Correlation between the dynamic pressure variation and the dynamic pressure value existing during the 10 min following the shock for events used in this study.

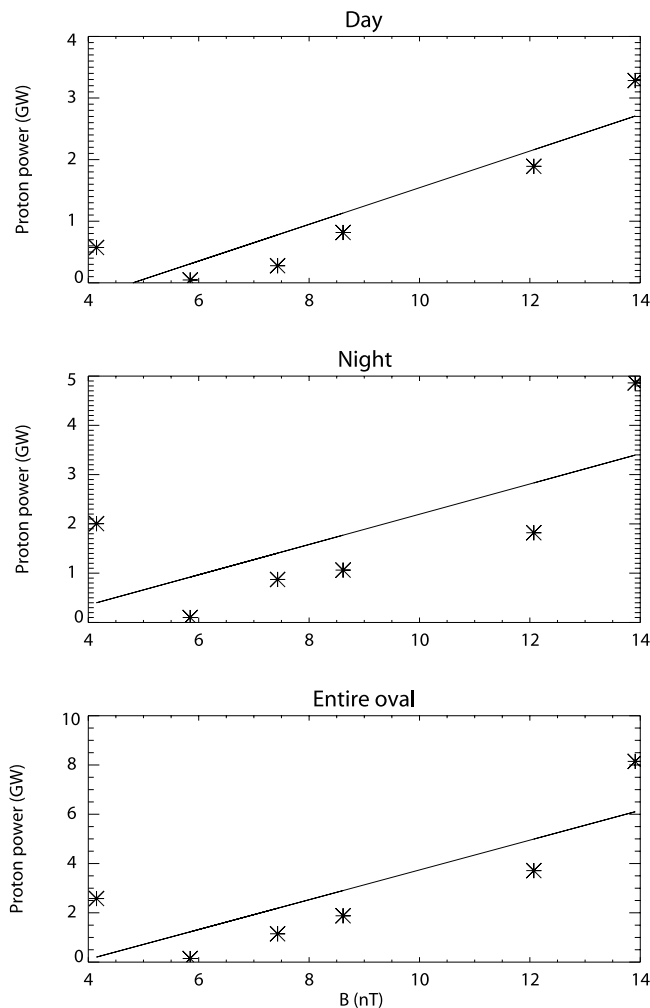


Figure 16. Correlation between the intensity of the magnetic field carried by the shock and proton auroral power for negative B_z events.

and proton rise times, which suggest mechanism acting identically on electrons and protons. The spatial resolution of the WIC and SI sensors does not permit to discriminate discrete from diffuse aurora, although, they show an intensification of the activity suggesting the development of diffuse aurora caused by adiabatic compression. In the nightside sector, as observed with the case study, even if the intensity of the activity observed in the nightside during shock events shows similarities with substorms, it also presents some differences. The nightside precipitation induced by shock is not always characterized by a localized onset following by eastward and/or westward travelling surges. Electron and proton precipitation are not necessarily collocated at the onset time, as in the case for auroral substorms [G erard *et al.*, 2004].

[43] The differential increase of the electron and proton power for both signs of B_z in the nightside region [Hubert *et al.*, 2002] explains the higher relative proton contribution to the HP in events occurring during a positive B_z period. On the dayside, plasma injection appears mostly as the result of the direct compression of the magnetosphere, which acts in parallel on electrons and protons. Consequently, the

relative contribution of protons is similar for positive and negative B_z events in the 1000–1700 MLT sector (the association of our defined noon and afternoon sectors).

[44] The relative proton contribution varies with the sector and the sign of B_z . The highest relative proton contribution is found in the afternoon sector and may be associated with clockwise (anticlockwise) drift of protons (electrons) coming from the tail, imply that they are first precipitated in the afternoon (morning) sector. It is also suggested that the larger temperature anisotropy existing in the afternoon sector may be at the origin of EMIC (electromagnetic ion cyclotron) waves responsible for the proton precipitation in this sector. The sign of B_z also influences the relative contribution of protons since the electron activity is more enhanced than the proton activity during southward IMF in the nightside sector. The dayside is also slightly influenced by the B_z orientation since it influences the temperature anisotropy.

[45] The correlation study also provides some clues to understand mechanisms occurring during shock events. The lack of correlation between the density of the SW plasma and the precipitation power suggests that the plasma injected during shock events is located inside the magnetosphere before the shock. The injected power is also independent of the dynamic pressure pulse but its arrival time at the front of the magnetosphere is closely linked with the triggering of the auroral precipitation. In this picture, the pressure pulse acts as a switch but the magnitude of the shock does not control the development of the aurora, at least for events due to the P_{dyn} variations of a factor of two in less than 15 min, the criteria used for this study. This lack of correlation with dynamic pressure and the solar wind density was also mentioned by Liou *et al.* [1998] for electron precipitation in a study which was not focused on shock induced aurora. The higher level of correlation of the injected powers with P_{dyn} for negative B_z events is presumably linked to a higher rate of reconnection between the Earth's magnetic field and the IMF during shock events.

[46] The control by the magnetic field intensity and the solar wind speed is consistent with the conclusions of Burch [1972], Akasofu and Chao [1980], Craven *et al.* [1986], Liou *et al.* [1998], and Boudouridis *et al.* [2003]. The SW-IMF control presents two distinct aspects as follows.

[47] 1. It has previously been shown that preconditioning of the magnetosphere mainly depends on the north-south orientation of the IMF during a period preceding the enhancement of activity. For our sample, the highest correlation coefficients with the values of B_z during the hour preceding the shock and the precipitated powers are surprisingly found in the dayside sector. However, these correlation coefficients are low (~ 0.36), which means a confidence level less than 50%. The preconditioning effect is more highlighted by the correlation between the sign of B_z (without the magnitude) and the precipitated power. The mean hemispheric power is 3 times more important when B_z is negative (~ 15 GW for negative B_z events 10 min after the shock and ~ 5 GW when B_z is positive) and this enhancement is mainly due to the nightside region. During positive B_z periods, the solar wind speed may also be considered as a preconditioning quantity. The correlation coefficient with the mean SW speed integrated over the hour preceding the

shock is $R = 0.45$ for electron HP and $R = 0.53$ for proton HP, i.e., a confidence level of $\sim 60\%$ and $\sim 70\%$, respectively. When B_z is negative, the precipitated powers seem independent of the SW speed (confidence level lower than 30%). Similarly to B_z and v , the value of the magnitude of the magnetic field (B) integrated on the hour preceding the shock is also weakly correlated with the precipitated power both for electron and proton precipitation independently of the sign of B_z . These correlations present a confidence level of $\sim 30\%$ ($R = 0.2$) except with the power due to proton in the dayside sector during positive B_z events, which presents a higher but still low confidence level (nearly the same as with the B_z component magnitude).

[48] 2. The solar wind and IMF conditions existing during the shock exerts also a rapid influence (time delay lower than 10 min) on the precipitated power. As presented in section 4.2, the most relevant quantities for this short time effect are B and v , which present the best correlations. The B_z quantity presents the same kind of correlation with the precipitated power integrated over a time period preceding or following the shock. As for the preconditioning effect, correlations between the magnitude of B_z and the precipitated powers are characterized by a relatively low confidence level. The highest confidence level is found in the dayside region when B_z is negative ($\sim 68\%$) and is around 50% for positive B_z periods. As for the preconditioning again, the comparison considering only the sign of B_z (constant before and after the shock for the events selected in this study) shows that auroral powers precipitated during negative B_z periods are 3 times more intense than during positive B_z .

[49] The preconditioning effect and the short time effect provide two different aspects of the magnetospheric reaction to a shock. B_z appears as the most influential parameter to organize the structure of the magnetosphere which will be perturbed by the arrival of the shock, whereas B , v , and B_z appear as factors determining the perturbation induced inside the magnetosphere by the shock. The short time influence of these quantities on auroral precipitation is confirmed by coupling functions giving the rate of energy transfer from the SW to the magnetosphere since these functions generally involve the solar wind speed and the magnetic field (as well as its north-south component) [Liou *et al.*, 1998]. The effect of B on shock aurora is probably linked to its influence on the magnetospheric configuration. The part of the oval most influenced by B may be linked with the location where reconnection occurs: at the front of the magnetosphere during southward B_z events and in the area of the magnetopause located above the poles during northward B_z events [Frey *et al.*, 2003]. Results presented in this study suggest that the solar wind speed also exerts some control on the injected power. From these results and the Liou *et al.* [1998] study, it is reasonable to believe that the origin of this control is thus the $\mathbf{B} \times \mathbf{v}$ solar wind electric field.

6. Conclusion

[50] The power induced by a shock on the magnetosphere and its longitudinal distribution was studied based on a set of 14 events observed with the IMAGE-FUV imagers. This set of events suggests that SW and IMF characteristics carried by the shock influences the induced precipitation

with a time delay lower than 10 min. The role of the preconditioning appears through the sign of the B_z component rather than its magnitude. The effect of preconditioning by the values of B and v existing before the shock appears less important on the power induced by the shock than the same quantities existing during the shock.

[51] In spite of common characteristics, auroral precipitation induced by shocks may be separated in two sets defined by the orientation of B_z when the shock occurs. The main similarity is the behavior observed in the 1400–1900 MLT sector suggesting the existence of mechanisms independent of the orientation of B_z acting in this region. Proton precipitation is the most important in this region, possibly as a consequence of temperature anisotropy and EMIC waves generation. Another similarity is the influence of the intensity of the magnetic field and the SW speed on the precipitated power for both signs of B_z . By contrast, the SW density and the dynamic pressure variation appear uncorrelated with the power due to electrons and protons.

[52] Some important differences are observed in the shock-induced power by both types of particles, the MLT distribution of auroral activity, and the influence of SW and IMF parameters. During negative B_z events, the auroral power injected in the ionosphere is higher than for positive B_z , especially on the nightside. Negative B_z shocks also induce an asymmetry about the noon-midnight axis in comparison with the distribution observed during positive B_z events. The relative proton contribution to the total power is lower during events with southward B_z , whereas the absolute power due to protons is higher than during positive B_z events but is not sufficient to compensate the dramatic increase of electron precipitation associated with negative B_z conditions. The magnetic field intensity influences the dayside region with a more important efficiency during southward B_z events and the nightside when B_z is positive even if, as mentioned above, B is a controlling factor of the entire oval. Our results also suggest an influence of B_z on the ability of the SW speed to influence electron precipitations.

[53] The lack of correlation with the SW density mentioned before confirms that the precipitated plasma is located inside the magnetosphere before the arrival of the shock. The influence of the sign of B_z existing before and after the shock on the energy transfer to the magnetosphere also confirm that reconnection plays an important role on the development of shock-induced aurora.

[54] **Acknowledgments.** J. C. Gérard and B. Hubert are supported by the Belgian Fund for Scientific Research (FNRS), and V. Coumans is supported by a fellowship from the Belgian Fund for Research in Industry and Agriculture (FRIA). The IMAGE-FUV investigation was supported by NASA through SWRI subcontract 83820 at the University of California, Berkeley, contract NAS5-96020. This research was partly funded by the PRODEX program of the European Space Agency. ACE level 2 data were provided by N. F. Ness (MFI) and D. J. McComas (SWEPAM) at the ACE science center. Dst indices are provided by the World Data Center for Geomagnetism (WDCG) in Kyoto (<http://swdcd.b.kugi.kyoto-u.ac.jp/dstdir/>). M. Meurant thanks N. Østgaard for assistance in the data presentation.

[55] Arthur Richmond thanks Athanasios Boudouridis and another reviewer for their assistance in evaluating this paper.

References

Akasofu, S.-I., and J. K. Chao (1980), Interplanetary shock waves and magnetospheric substorms, *Planet. Space Sci.*, 28, 381.

- Boudouridis, A., E. Zesta, L. R. Lyons, P. C. Anderson, and D. Lummerzheim (2003), Effect of solar wind pressure pulses on the size and strength of the auroral oval, *J. Geophys. Res.*, *108*(A4), 8012, doi:10.1029/2002JA009373.
- Brown, R. R., T. R. Hartz, B. Landmark, H. Leinbach, and J. Ortner (1961), Large-scale electron bombardment of the atmosphere at the sudden commencement of a geomagnetic storm, *J. Geophys. Res.*, *66*, 1035.
- Burch, J. L. (1972), Preconditions for the triggering of polar magnetic substorms by storm sudden commencements, *J. Geophys. Res.*, *77*, 5629.
- Chua, D., G. Parks, M. Brittner, W. Peria, G. Germany, J. Spann, and C. Carlson (2001), Energy characteristics of auroral electron precipitation: A comparison of substorms and pressure pulse related auroral activity, *J. Geophys. Res.*, *106*, 5945.
- Coumans, V., J.-C. Gérard, B. Hubert, M. Meurant, and S. B. Mende (2004), Global auroral conductance distribution due to electron and proton precipitation from IMAGE-FUV observations, *Ann. Geophys.*, *22*, 1595.
- Craven, J. D., L. A. Franck, C. T. Russell, E. J. Smith, and R. P. Lepping (1986), Global auroral response to magnetospheric compression by shocks in the solar wind: Two case studies, in *Solar Wind-Magnetosphere Coupling*, edited by Y. Kamide and J. A. Slavin, pp. 377–380, Terra Sci., Tokyo.
- Frey, H. U., S. B. Mende, T. J. Immel, S. A. Fuselier, E. S. Clafin, J.-C. Gérard, and B. Hubert (2002), Proton aurora in the cusp, *J. Geophys. Res.*, *107*(A7), 1091, doi:10.1029/2001JA900161.
- Frey, H. U., T. D. Phan, S. A. Fuselier, and S. B. Mende (2003), Continuous magnetic reconnection at Earth's magnetopause, *Nature*, *426*(6966), 533.
- Gérard, J.-C., B. Hubert, A. Grard, M. Meurant, and S. B. Mende (2004), Solar wind control of auroral substorm onset locations observed with the IMAGE-FUV imagers, *J. Geophys. Res.*, *109*, A03208, doi:10.1029/2003JA010129.
- Glassmeier, K. H., and C. Heppner (1992), Traveling magnetospheric convection twin-vortices: Another case study, global characteristics, and a model, *J. Geophys. Res.*, *97*, 3977.
- Haerendel, G. (1994), Acceleration from field-aligned potential drops, *Astrophys. J. Suppl. Series*, *90*, 765.
- Hardy, D. A., M. S. Gussenhoven, and D. Brautigam (1989), A statistical model of auroral ion precipitation, *J. Geophys. Res.*, *94*, 370.
- Heppner, J. P. (1955), Note on the occurrence of world-wide ssc's during the onset of negative bays at College, *J. Geophys. Res.*, *60*, 29–32.
- Hubert, B., J. C. Gérard, D. S. Evans, M. Meurant, S. B. Mende, H. U. Frey, and T. J. Immel (2002), Total electron and proton energy input during auroral substorms: Remote sensing with IMAGE-FUV, *J. Geophys. Res.*, *107*(A8), 1183, doi:10.1029/2001JA009229.
- Hubert, B., J. C. Gérard, S. A. Fuselier, and S. B. Mende (2003), Observation of dayside subauroral proton flashes with the IMAGE-FUV imagers, *Geophys. Res. Lett.*, *30*(3), 1145, doi:10.1029/2002GL016464.
- Immel, T. J., J. D. Craven, and A. C. Nicholas (2000), An empirical model of the OI FUV dayglow from DE-1 images, *J. Atmos. Sol. Terr. Phys.*, *62*, 47.
- Kawasaki, K., S.-I. Akasofu, F. Yasuhara, and C.-I. Meng (1971), Storm sudden commencements and polar magnetic substorms, *J. Geophys. Res.*, *76*, 6781.
- Kokubun, S., R. L. McPherron, and C. T. Russell (1977), Triggering of substorms by solar wind discontinuities, *J. Geophys. Res.*, *82*, 74.
- Liou, K., P. T. Newell, C.-I. Meng, M. Brittner, and G. Parks (1998), Characteristics of the solar wind controlled auroral emissions, *J. Geophys. Res.*, *103*, 17,543.
- Liou, K., P. T. Newell, D. G. Sibeck, C. I. Meng, M. Brittner, and G. Parks (2001), Observation of IMF and seasonal effects in the location of auroral substorms, *J. Geophys. Res.*, *106*, 5799.
- Liou, K., P. T. Newell, C.-I. Meng, C.-C. Wu, and R. P. Lepping (2002), Do interplanetary shocks really trigger substorm expansion phase onsets?, in *Sixth International Conference on Substorms*, edited by R. M. Winglee, p. 299, Univ. of Wash., Seattle, Wash.
- Liou, K., P. T. Newell, C.-I. Meng, C.-C. Wu, and R. P. Lepping (2003), Investigation of external triggering of substorms with Polar ultraviolet imager observation, *J. Geophys. Res.*, *108*(A10), 1364, doi:10.1029/2003JA009984.
- Lummerzheim, D., M. Brittner, D. Evans, G. A. Germany, G. K. Parks, M. H. Rees, and J. F. Spann (1997), High time resolution study of the hemispheric power carried by energetic electrons into the ionosphere during the May 19/20, 1996 auroral activity, *Geophys. Res. Lett.*, *24*, 987.
- Matsushita, S. (1961), Increase of ionization associated with geomagnetic sudden commencements, *J. Geophys. Res.*, *81*, 2289.
- Mende, S. B., et al. (2000), Far ultraviolet imaging from the IMAGE spacecraft: 2. Wideband FUV imaging, *Space Sci. Rev.*, *91*, 271.
- Meurant, M., J.-C. Gérard, B. Hubert, V. Coumans, V. I. Shematovich, D. V. Bisikalo, D. S. Evans, G. R. Gladstone, and S. B. Mende (2003a), Characterization and dynamics of the auroral electron precipitation during substorms deduced from IMAGE-FUV, *J. Geophys. Res.*, *108*(A6), 1247, doi:10.1029/2002JA009685.
- Meurant, M., J.-C. Gérard, B. Hubert, C. Blockx, N. Østgaard, and S. B. Mende (2003b), Dynamics of global scale electron and proton precipitation induced by a solar wind pressure pulse, *Geophys. Res. Lett.*, *30*(20), 2032, doi:10.1029/2003GL018017.
- Nishida, A. (1978), *Geomagnetic Diagnosis of the Magnetosphere*, Springer-Verlag, New York.
- Ortner, J., B. Hultqvist, R. R. Brown, T. R. Hartz, O. Holt, B. Landmark, J. L. Hook, and H. Leinbach (1962), Cosmic noise absorption accompanying geomagnetic storm sudden commencement, *J. Geophys. Res.*, *67*, 4169.
- Østgaard, N., G. Germany, J. Stadsnes, and R. R. Vondrak (2002), Energy analysis of substorms based on remote sensing techniques, solar wind measurements, and geomagnetic indices, *J. Geophys. Res.*, *107*(A9), 1233, doi:10.1029/2001JA002002.
- Press, W. H., B. P. Flannery, S. A. Teukolsky, and W. T. Vetterling (1989), *Numerical Recipes: The Art of Scientific Computing, FORTRAN Version*, Cambridge Univ. Press, New York.
- Schildge, J. P., and G. L. Siscoe (1970), A correlation of the occurrence of simultaneous sudden magnetospheric compression and geomagnetic bay onsets with selected geophysical indices, *J. Atmos. Terr. Phys.*, *32*, 1819.
- Siscoe, G. L., N. U. Crooker, and K. D. Siebert (2002), Transpolar potential saturation: Roles of region 1 current system and solar wind ram pressure, *J. Geophys. Res.*, *107*(A10), 1321, doi:10.1029/2001JA009176.
- Song, Y., and R. L. Lysak (1989), Evaluation of twist helicity in FTE flux tubes, *J. Geophys. Res.*, *94*, 5273.
- Southwood, D. J., and M. G. Kivelson (1990), The magnetohydrodynamic response of the magnetospheric cavity to changes in solar wind pressure, *J. Geophys. Res.*, *95*, 2301.
- Tsurutani, B. T., et al. (2001), Auroral zone dayside precipitation during magnetic storm initial phases, *J. Atmos. Sol. Terr. Phys.*, *63*, 513.
- Ullaland, S. L., K. Wilhem, J. Kanges, and W. Reidler (1970), Electron precipitation associated with a sudden commencement of a geomagnetic storm, *J. Atmos. Terr. Phys.*, *32*, 1545.
- Vorob'yev, V. G. (1974), Sc-associated effects in auroras, *Geomagn. Aeron.*, *14*, 72.
- Zhou, X.-Y., and B. T. Tsurutani (1999), Rapid intensification and propagation of the dayside aurora: Large scale interplanetary pressure pulses (fast shocks), *Geophys. Res. Lett.*, *26*, 1097.
- Zhou, X.-Y., and B. T. Tsurutani (2001), Interplanetary shock triggering of night-side geomagnetic activity: Substorms, pseudobreakups, and quiet events, *J. Geophys. Res.*, *106*, 18,957.
- Zhou, X.-Y., R. J. Strangeway, P. C. Anderson, D. G. Sibeck, B. T. Tsurutani, G. Haerendel, H. U. Frey, and J. K. Arballo (2003), Shock aurora: FAST and DMSP observations, *J. Geophys. Res.*, *108*(A4), 8019, doi:10.1029/2002JA009701.

C. Blockx, V. Coumans, J.-C. Gérard, B. Hubert, and M. Meurant, Laboratoire de Physique Atmosphérique et Planétaire, Université de Liège, B-4000 Liège-Ougrée, Belgium. (mmeurant@ulg.ac.be)